Mon. Not. R. Astron. Soc. **000**, 1–?? (2002) Printed 24 October 2014 (MN LATEX style file v2.2)

Chemical modeling of water deuteration in IRAS16293-2422

V. Wakelam[1,2⋆], C. Vastel[3,4], Y. Aikawa[5], A. Coutens[6,7], S. Bottinelli[3,4], E. Caux[3,4]
[1] *Univ. Bordeaux, LAB, UMR 5804, F-33270, Floirac, France*
[2] *CNRS, LAB, UMR 5804, F-33270, Floirac, France*
[3] *Université de Toulouse; UPS-OMP; Institut de Recherche en Astrophysique et Planétologie (IRAP) ; UMR 5277 ; Toulouse, France*
[4] *CNRS; IRAP; UMR 5277 ; 9 Av. colonel Roche, BP 44346, F-31028 Toulouse cedex 4, France*
[5] *Department of Earth and Planetary Sciences, Kobe University, Kobe 657-8501, Japan*
[6] *Niels Bohr Institute, University of Copenhagen, Juliane Maries Vej 30, DK-2100 Copenhagen Ø, Denmark*
[7] *Centre for Star and Planet Formation and Natural History Museum of Denmark, University of Copenhagen, Øster Voldgade 5-7, DK-1350 Copenhagen K., Denmark*

arXiv:1410.6366v1 [astro-ph.GA] 23 Oct 2014

xx

ABSTRACT

IRAS 16293-2422 is a well studied low-mass protostar characterized by a strong level of deuterium fractionation. In the line of sight of the protostellar envelope, an additional absorption layer, rich in singly and doubly deuterated water has been discovered by a detailed multiline analysis of HDO. To model the chemistry in this source, the gas-grain chemical code Nautilus has been used with an extended deuterium network. For the protostellar envelope, we solve the chemical reaction network in infalling fluid parcels in a protostellar core model. For the foreground cloud, we explored several physical conditions (density, cosmic ionization rate, C/O ratio).
The main results of the paper are that gas-phase abundances of H_2O, HDO and D_2O observed in the inner regions of IRAS16293-2422 are lower than those predicted by a 1D dynamical/chemical (hot corino) model in which the ices are fully evaporated. The abundance in the outer part of the envelope present chaotic profiles due to adsorption/evaporation competition, very different from the constant abundance assumed for the analysis of the observations. We also found that the large abundances of gas-phase H_2O, HDO and D_2O observed in the absorption layer are more likely explained by exothermic surface reactions rather than photodesorption processes.

Key words: Astrochemistry – stars: protostars – ISM: abundances – ISM: molecules – ISM: IRAS16293-2422 .

1 INTRODUCTION

Water in the interstellar medium has been widely observed and analyzed in the past few years thanks to the success of the Herschel Space Observatory (Pilbratt et al. 2010) and the high spectral resolution of its Heterodyne Instrument for the Far-Infrared (de Graauw et al. 2010). It has been detected in various environments like comets (Hartogh et al. 2011; Bockelée-Morvan et al. 2012), low-mass star-forming regions (Kristensen et al. 2012), high-mass star-forming regions (van der Tak et al. 2013), protoplanetary disks (Podio et al. 2013) and one prestellar core (Caselli et al. 2012). See van Dishoeck et al. (2013) for a full review on interstellar water. Water can be formed in the gas-phase, mostly by ion-molecular reactions starting from the atomic oxygen and ending with the dissociative recombination of H_3O^+ in dense regions but it is most efficiently formed at the surface of interstellar grains by the successive hydrogenation of atomic and molecular oxygen (Miyauchi et al. 2008; Dulieu et al. 2010; Ioppolo et al. 2010; Cuppen et al. 2010). Water ice formation starts at a threshold extinction of $A_V \sim$ 3-5 magnitudes, well before the cloud collapses (Whittet 1993; Hartquist 2003).
In very cold regions, a small fraction of the H_2O ice formed by surface reactions can be desorbed back into the gas phase through non-thermal processes. For example the cosmic rays have the ability to penetrate even the densest clouds and therefore maintain a low level of UV radiation by interacting with molecular hydrogen. The indirect cosmic ray induced desorption is then an important mechanism (Leger et al. 1985; Hasegawa & Herbst 1993). In the same way, the far UV starlight pervading interstellar space photodesorbs water molecules from grains in dense regions well below the evaporation temperature (Hollenbach et al. 2009). The efficiency of the photodesorption has been quantified by laboratory experiments to be $\sim 10^{-3}$ per incident UV photon with a dependence on the ice thickness and temperature (Öberg et al. 2009). Similar results were found theoretically by Andersson et al. (2006) and Andersson & van Dishoeck (2008). In particular, the detection of water vapor inside pre-stellar cores seems to indicate that the photo evaporation processes of the ices by the cosmic-ray

⋆ E-mail: wakelam@obs.u-bordeaux1.fr

induced FUV photons can be efficient (Caselli et al. 2012).
The start of the collapse of a cloud triggers the increase of luminosity at the centre of the protostellar object, which eventually increases the temperatures well above 100 K, then H_2O ices are thermally desorbed on very short timescales (Fraser et al. 2001). This evaporation results in **theoretical** gas-phase abundances of H_2O as high as $\sim 10^{-4}$, relative to hydrogen. Together with water, other species desorb at the same time characterizing these hot cores (in the case of high-mass young stellar objects) or hot corinos (in the case of low-mass young stellar objects). Other regions in star forming regions associated with shocks (created by the interaction of molecular outflows with the quiescent surrounding cloud) show large enhancement of H_2O abundances due to temperatures of several thousand degrees Kelvin. Detection of cold water vapor in a disk around the young star TW Hydrae suggests a water ice reservoir equivalent up to several thousand Earth oceans in mass, with implications on the origin of our Earth's oceans (Hogerheijde et al. 2011).
Water deuteration is unique compared to other species. In the first stages of star formation, low temperatures and the disappearance of most molecules, and particularly of CO, from the gas phase trigger a peculiar chemistry (Millar et al. 1989). An extreme molecular deuteration has been extensively discovered over the past 10 years in dense prestellar cores and low-mass protostars, with deuteration fractionation as high as 100% (see Ceccarelli et al. 2014, PP6, for a review). The D/H ratio of interstellar water ice is, however, not well constrained. HDO ice has not been detected, and upper limits in the range from 0.002 to 0.02 have been estimated in protostar samples (Dartois et al. 2003; Parise et al. 2003; Aikawa et al. 2012). Since water ice is sublimated to the gas phase in hot corinos, gas-phase HDO has been extensively investigated in recent years (Coutens et al. 2012; Taquet et al. 2013; Jørgensen & van Dishoeck 2010a). The deuteration fraction of water is much lower (less than 1%) for both high-mass and low-mass protostars than for other species that show sometimes a D/H ratio several orders of magnitude higher compared to the cosmic value. Furthermore, no HDO has been detected yet in the prestellar core phase, although many deuterated species appear with a high deuteration fractionation (Phillips & Vastel 2003; Vastel et al. 2004). **If deuterated water is mostly formed by surface reactions, the level of deuteration of water may be much lower compared to other species formed in the gas-phase in cold dense clouds (Roberts et al. 2003). Comparing the HDO/H_2O ratios observed in protostellar envelopes to the ones in comets and the Earth's oceans (with a Vienna Standard Mean Ocean Water value of 1.558×10^{-4}) could bring new insight on the origin of water and life on planets.** The recent observations of a Jupiter-family comet is consistent with the VSMOW value, suggesting that the ocean water could have been delivered by these external sources.

We concentrate, in this paper, on water vapor in the IRAS 16293-2422 low-mass protostar (hereafter IRAS16293), which remains the first source in which doubly-deuterated water has been detected (Butner & Charnley 1997; Vastel et al. 2010) and towards which the most complete study of water and deuterated water has been performed to date (Coutens et al. 2012, 2013). Observed data for 16 HDO, 7 para-$H_2^{18}O$, 8 ortho-$H_2^{18}O$, 1 ortho- and 1 para-$H_2^{17}O$, 1 $HD^{18}O$, 1 ortho-D_2O and 2 para-D_2O transitions have been used simultaneously with the spherical Monte Carlo radiative transfer code RATRAN (Hogerheijde & van der Tak 2000) assuming an abundance jump at 100 K (Fraser et al. 2001), which corresponds to an approximate radius of 70 AU. A water-rich absorbing layer is required in front of the envelope to reproduce the HDO absorption components observed at 465 and 894 GHz. Coutens et al. (2012) proposed that this layer results from the photodesorption of water ice induced by the external UV radiation field, as predicted by Hollenbach et al. (2009) in molecular clouds at a visual extinction, A_V, between 1 and 4. The only physical constraints on this foreground cloud is that the temperature is lower than 30 K and the H_2 density lower than 10^5 cm^{-3}. The observed abundances in the different components in the line of sight of the protostar are summarized in Table 1. Note that for the foreground cloud, we have only reported abundances computed assuming A_V of 3 and 4 since we show in this paper that at smaller A_V the model predicts very low abundances.
The present paper aims at studying the deuteration of water in the envelope of IRAS16293 and the foreground cloud in order to reproduce the observed large abundances of deuterated water. The model (with a different network) and approach used in this paper are the same as in Bottinelli et al. (2014) for the analysis of CH lines in the line of sight of IRAS16293. The modeling for the two different components is presented in separate sections: Section 2 for the protostellar envelope and Section 3 for the foreground cloud. In each of the two sections, the model is first presented. Then the model results are shown with some studies of the results sensitivity to the model parameters. In Section 4, we discuss the effect of a number of parameters and the efficiency of the photo evaporation processes in the foreground cloud. We conclude in the last section.

2 THE PROTOSTELLAR ENVELOPE

2.1 Chemical and physical model description

2.1.1 The Nautilus chemical model

To theoretically study the deuteration of water in the envelope of IRAS16293, the chemical model Nautilus has been used with the spherical protostellar core model similar to Aikawa et al. (2008, 2012) (see section 2.1.3). Nautilus is a chemical model that computes the evolution of the species abundances as a function of time in the gas-phase and at grain surfaces. The code has been used for a variety of environments such as dense clouds (Loison et al. 2014), low mass protostellar envelopes (Bottinelli et al. 2014) and the outer regions of protoplanetary disks (Dutrey et al. 2011). A large number of gas-phase processes are included in the network: bimolecular reactions (between neutral species, between charged species and between neutral and charged species) and unimolecular reactions, i.e. photo reactions with direct UV photons and UV photons produced by the deexcitation of H_2 excited by cosmic-ray particles (Pratap & Tarafdar mechanism), and direct ionization and dissociation by cosmic-ray particles. The interactions of the gas-phase species with the interstellar grains are: sticking of neutral gas-phase species to the grain surfaces, evaporation of the species from the surfaces due to the temperature, the cosmic-ray heating and the exothermicity of the reactions at the surface of the grains. The species can diffuse and undergo reactions using the rate equation approximation at the surface of the grains (Hasegawa et al. 1992). Details on the processes included in the model can be found in Semenov et al. (2010) and Loison et al. (2014).

Table 1. Observed abundance of H_2O, HDO and D_2O towards the line of sight of IRAS16293 from Coutens et al. (2013).

	Hot corino (r ⩽ 75 AU)	Outer envelope (r > 75 AU)	foreground cloud* (A_V = 4 - 3)
H_2O	$4.7 - 40 \times 10^{-6}$	$7.0 - 22.5 \times 10^{-9}$	$1.3 - 1.8 \times 10^{-7}$
HDO	$1.4 - 2.4 \times 10^{-7}$	$5.5 - 10.6 \times 10^{-11}$	$6 - 8 \times 10^{-9}$
D_2O	$\leqslant 1.3 \times 10^{-9}$	$\leqslant 1.3 \times 10^{-11}$	$6.6 - 8.9 \times 10^{-10}$
HDO/H_2O	$4 \times 10^{-3} - 5.1 \times 10^{-2}$	$3 \times 10^{-3} - 1.5 \times 10^{-2}$	$\sim 4 \times 10^{-2}$
D_2O/HDO	$\leqslant 9 \times 10^{-3}$	$\leqslant 0.23$	~ 0.11
D_2O/H_2O	$\leqslant 3 \times 10^{-4}$	$\leqslant 2 \times 10^{-3}$	$\sim 5 \times 10^{-3}$

* The abundances are given for A_V = 4 and 3 respectively.

2.1.2 *The deuterated network*

We adopt the reaction network model of Aikawa et al. (2012), which we briefly describe in the following. Aikawa et al. (2012) extended the gas-grain reaction network of Garrod & Herbst (2006) to include mono-, doubly-, and triply-deuterated species. The reaction rate coefficients of deuterated species are set to be the same as that of the original reactions (Garrod & Herbst 2006). If there are more than one set of possible products (e.g. XH+YD and XD+YH), statistical branching ratio is assumed. Reactions listed in Millar et al. (1989) and Roberts et al. (2004) are included in the network; these are mostly exchange reactions that trigger the isotopic fractionation.

At temperatures up to several tens of Kelvin, deuterium fractionation is mainly triggered by an exothermic exchange reaction $H_3^+ + HD \rightarrow H_2D^+ + H_2$ and its multi-deuterated analogues. Since the reactions are exothermic, the backward reaction is much less efficient, and H_3^+ is highly deuterated. Since CO is the main reactant of H_2D^+, CO depletion in prestellar cores further enhances the D/H ratio of H_3^+ (Vastel et al. 2003). However, such enhancement can be limited by ortho-H_2, which can react with the deuterated trihydrogen cation and remove the deuterium. Indeed, the 170K internal energy of the lowest ortho-H_2 level (J=1) is large compared to the temperatures considered in the cold medium and reactions which are endothermic with para-H_2 can have much smaller endothermicity with ortho-H_2. Considering the complexity of the network, we did not consider the ortho, para or meta forms of any species. We discuss the importance of this approximation in section 4.4.

In molecular clouds, water is mainly formed via three chemical paths. The first path is a series of ion-molecule reactions and recombination:

$$O + H_3^+ \rightarrow OH^+ + H_2 \quad (1)$$

$$OH^+ + H_2 \rightarrow H_2O^+ + H \quad (2)$$

$$H_2O^+ + H_2 \rightarrow H_3O^+ + H \quad (3)$$

$$H_3O^+ + e \rightarrow H_2O + H \quad (4)$$

If deuterated H_3^+, e.g. H_2D^+, reacts with O atom in the first step (reaction 1), HDO can be formed with a statistical branching ratio. The D/H ratio of water formed by this ion-molecule path is similar to (although slightly smaller than) that of H_3^+.
The second path is a hydrogenation of O atom on grain surface:

$$O + H \rightarrow OH \quad (5)$$

$$OH + H \rightarrow H_2O \quad (6)$$

The recombination of deuterated H_3^+ enhances the atomic D/H ratio in the gas phase. These atoms then collide with grains and participate in the hydrogenation on grain surfaces. Water formed on grains are thus deuterated as well.
The third path is neutral-neutral reactions in the gas-phase:

$$O + H_2 \rightarrow OH + H \quad (7)$$

$$OH + H_2 \rightarrow H_2O + H \quad (8)$$

These reactions are endothermic by ~ 3000 K for the first one and exothermic but with an activation barrier of ~ 1000 K for the second one, and thus are efficient only at temperatures higher than a few hundred K.

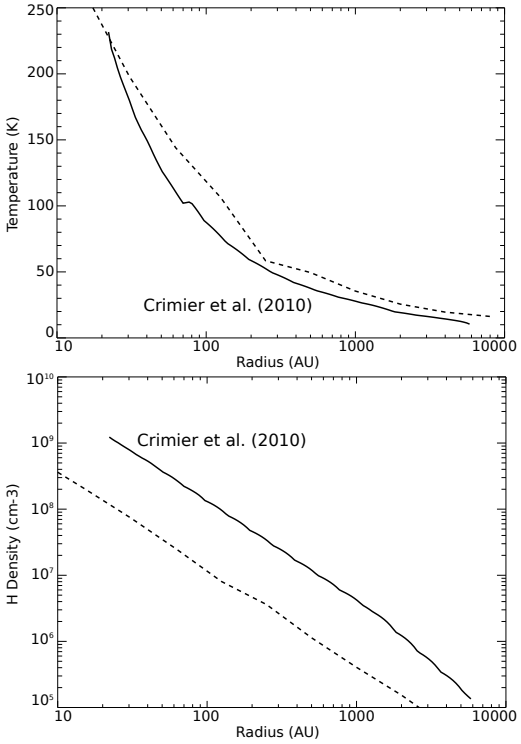

Figure 1. Temperature and density profiles in the protostellar envelope. The dashed curve represents the protostellar core model from Masunaga & Inutsuka (2000) and the solid one the profiles derived by Crimier et al. (2010) in the envelope of IRAS16293-2422.

2.1.3 *The protostellar physical model*

As in Aikawa et al. (2008, 2012), the physical structure is based on the radiation hydrodynamical model from Masunaga & Inutsuka (2000). The model starts from the dense molecular cloud core with a central density of $n(H_2) \sim 3 \times 10^4$ cm^{-3}. The core extends to

$r = 4 \times 10^4$ AU, and the total mass is 3.852 $M_\odot$. The contraction is almost isothermal as long as the cooling is efficient. Eventually the compressional heating overwhelms the cooling, and the temperature rises in the central region. Then the core goes through the first core stage and second collapse to form a protostar at the center. In the model we adopt, the prestellar core evolves to the protostellar core in 2.5×10^5 yr. After the birth of the protostar, the model further follows the evolution for 9.3×10^4 yr, during which the protostar grows by mass accretion from the envelope.

The physical structure of the envelope at the final time of the simulation (9.3×10^4 yr) are similar to the one constrained in the envelope of IRAS16293 by Crimier et al. (2010) from multi-wavelenght dust and molecular observations. Fig. 1 shows a comparison between the model of Masunaga & Inutsuka (2000) and observed temperature and density profiles as a function of radius. The temperature profiles are quite similar whereas the observed density profile is about ten times larger in the calculated one. To better match the observations and be consistent with the profile used to interpret the observations, we have multiplied by 10 all the densities in our simulations. The consequences of this modification of the physical model are discussed in section 4.5.

2.1.4 Model parameters

The chemical composition is computed using the physical structure previously described. Each cell of material is assumed to be independent so that there is no mixing between cells. In total, there are 15 different cells that are allowed to dynamically evolve and which defines the physical and chemical structure of the envelope from 0.66 AU up to 8000 AU at the final time. As in Aikawa et al. (2008, 2012), we assume that the object is embedded in a molecular cloud so that the minimum A_V at the border of the envelope is approximately 4. To obtain the chemical composition prior to the collapse, we compute the chemistry, using the local physical conditions in a pre stellar dense core, for 10^6 yr as in Aikawa et al. (2008). Note that the density at this stage is also multiplied by a factor of 10. For this first step, the species are assumed to be initially in the atomic form, except for the hydrogen and the deuterium. The hydrogen is initially molecular H_2 and deuterium in the form of HD. The elemental abundances used for the simulations are the same as in Hincelin et al. (2011), with an oxygen elemental abundance of 3.3×10^{-4} (compared to the total H density, which gives a C/O elemental ratio of 0.5). The deuterium elemental abundance is set to 1.5×10^{-5} compared to H, which is the average value found by absorption spectroscopy measurements towards stars in the vicinity of the Sun (e.g. Linsky et al. 2006). The cosmic-ray ionization rate is 1.3×10^{-17} s^{-1}, typical value used in chemical modeling and found in dense clouds (Caselli et al. 1998).

In addition to this standard model, we have explored the importance of the three following parameters: the age of the parent cloud (Parameter 1: P1), the oxygen elemental abundance (P2) and the cosmic-ray ionization rate (P3). Instead of running the code for 10^6 yr (P1) before the collapse, we run it for 10^4 and 10^5 yr. For the oxygen elemental abundance (P2), we also considered an abundance of 1.4×10^{-4} (corresponding to a C/O of 1.2). Finally, for the cosmic-ray ionization rate (P3), we used a ten times larger value of 10^{-16} s^{-1}, more typical of diffuse clouds observations (Indriolo & McCall 2012) but proposed by Doty et al. (2004) for the envelope of IRAS16293. All the parameters, which impact on the model predictions have been studied, are summarized in Table 2.

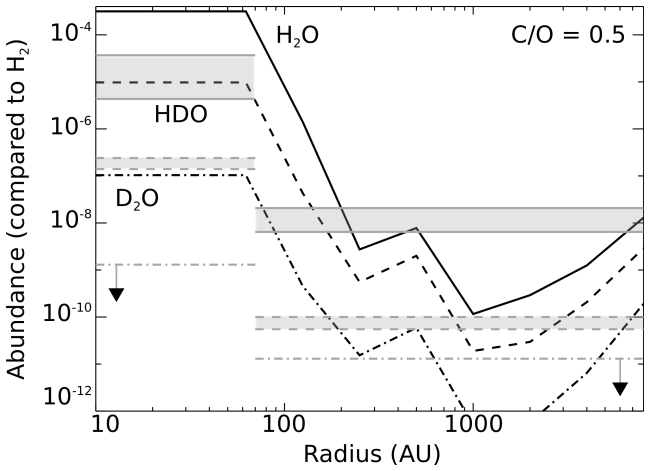

Figure 2. Abundance profiles, in the gas-phase, of H_2O (solid line), HDO (dashed line) and D_2O (dash-dotted line) predicted by the standard model towards the envelope of IRAS16293. Grey lines and areas represent the observational constraints. Constraints on D_2O abundance are only upper limits.

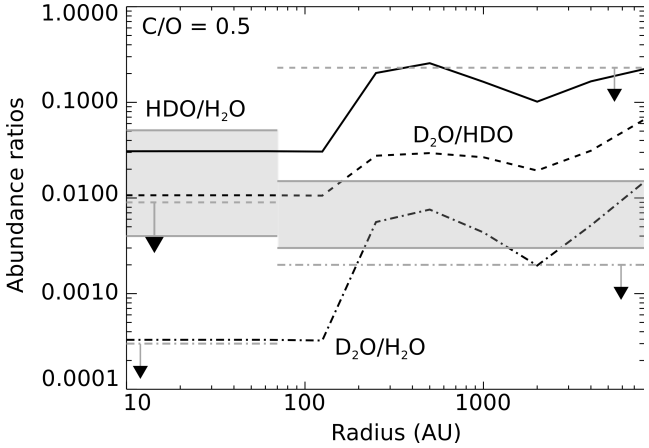

Figure 3. HDO/H_2O (solid line), D_2O/H_2O (dash-dotted line) and D_2O/HDO (dashed line) abundance ratios as a function of radius towards the center of the protostellar envelope predicted by the standard model. Grey lines and areas represent the observational constraints (only upper limits for D_2O/HDO and D_2O/H_2O).

2.2 Modeling results

In this section, we present the predicted abundances for water and its deuterated forms in the envelope of IRAS16293 for the standard model, and compare them with the observed values. Note that the radius, at which the temperature is 100 K, defines the limit between the inner and outer regions of the protostar for the analysis of the observations. In Coutens et al. (2012), they have used the radius of 75 AU from Crimier et al. (2010). In our simulations, it would be 70 AU and we have chosen to use this value to plot the observed abundances on the figures. Fig. 2 shows the calculated abundances of H_2O, HDO and D_2O in the protostellar envelope as a function of radii, at the end of the simulations, i.e. for a protostellar age of 9.3×10^4 yr. The gas-phase abundances of these species predicted by the model can be divided in three regions. The first one is defined by radii larger than 1000 AU and temperatures below 30 K. In this region, the gas-phase abundances decrease towards the center of the envelope due to the depletion of species because

Table 2. Parameters of the chemical model explored for the 1D model of the protostellar envelope and the 0D model of the foreground cloud

1D Modeling of the protostellar envelope	
Parameters of the standard model	
Density structure	$10 \times$ density computed by the MHD model
Free-fall timescale	Timescale computed by the MHD model
Time before collapse	10^6 yr
Parameters tested	
Density structure	Density computed by the MHD model (section 4.5)
Free-fall timescale	Timescale computed by the MHD model / 3 (section 4.5)
Time before collapse	10^4 and 10^5 yr (section 2.4)
0D Modeling for the foreground cloud	
Gas and dust temperature	15 and 30 K
H density	2×10^4 and 2×10^5 cm^{-3}
Visual extinction	2, 3 and 4
Parameters tested for both 0D and 1D modelings	
Cosmic-ray ionization rate	10^{-17} and 10^{-16} s^{-1}
C/O elemental ratio	0.5 and 1.2
Deuterium elemental abundance	7.5×10^{-6}, 1.5×10^{-5}, 3×10^{-5}
Rate coefficient of the reaction $H_2D^+ + H_2 \rightarrow H_3^+ + HD$	see section 4.4

of the density increase. Between 1000 and about 70 AU, the gas-phase abundances increase. The cause of this increase is first the thermal desorption of precursors such as HDCO and H_2CO from the ices that react with OH and OD between 1000 and 250 AU (where the temperature is between 30 and 60 K). The second cause is the direct thermal evaporation of H_2O, HDO and D_2O from the mantles until complete evaporation at between 250 and 70 AU (where the temperature is between 60 and 100 K). The last region is defined by radii smaller than 70 AU where the gas-phase abundances are constant. In fact the inner abundances are equal to the abundances in the ices that are constant across the envelope before the collapse since H_2O formation and deuteration occurs at the surface of the grains during this phase. At the protostellar stage, the ice abundance of these species stays constant for radii larger than 70 AU. Contrary to Mottram et al. (2013), we have a smoother increase of the water gas-phase abundance towards the center of the protostar. The main difference with their work is that we are using a dynamical structure rather than a static one. In a static model, the gas and dust stay at the same radius and physical conditions for the entire time of the collapse. The depletion of molecules is then more important than in a dynamical model in which each cell of material stays less longer at high density. In addition, Mottram et al. (2013) have used a simplified chemistry to compte the abundance of water, which very likely does not include the gas-phase formation of H_2O from H_2CO evaporated from the ices.

2.3 Comparison with the observations

Compared to the observations (Coutens et al. 2013), the most inner abundances are over-predicted by the chemical model, in particular for D_2O (see Fig. 2). This disagreement could be explained by the uncertainties on the structure of Crimier et al. (2010), which is not constrained at small scale ($\lesssim$ 500 AU). The abundances are however nicely reproduced for the three molecules for a radius of 90 to 100 AU, which could suggest that water is not totally desorbed in the inner regions. This could be expected in case of the presence of a disk, as most of the molecules are assumed to be trapped on the grain mantles in the cold midplane layer of the disk. In particular, Pineda et al. (2012) suggested that a disk would surround the source A. The determination of the disk properties (H_2 density, temperature) would then be required in order that this 2D or 3D structure can be taken into account both to derive the observed abundances and to predict the chemical abundances. This would enable a more reliable comparison between the observations and the chemical predictions. Note that the water abundances predicted by our chemical model in the gas-phase (which results for the ice evaporation) are in agreement with the abundances of H_2O observed in the ices of about 10^{-4} (Schutte et al. 1996). Fig. 3 shows the abundance ratios HDO/H_2O, D_2O/H_2O and D_2O/HDO predicted by the model as well as the observational constraints derived by Coutens et al. (2013). Abundance ratios in the inner region of the envelope are satisfactory reproduced by the model. A low HDO/H_2O ratio ($9.2 \pm 2.6 \times 10^{-4}$) was however recently derived in the inner regions of IRAS16293, based on interferometric data of the HDO line at 226 GHz and the $H_2{}^{18}O$ lines at 203 and 692 GHz (Persson et al. 2013), closer to the lower value of the ratio determined by Coutens et al. (see Table 1). The difference between the HDO/H_2O ratios derived by Coutens et al. (2013) and Persson et al. (2013) could be due to the optically thickness of some $H_2^{18}O$ lines observed with *Herschel*/HIFI (Visser et al. 2013). Other low-mass protostars (NGC1333 IRAS4A, IRAS4B and IRAS2A) seem to show a similar HDO/H_2O ratios of $\sim 10^{-3}$ in the warm inner regions (Visser et al. 2013; Coutens et al. 2013; Persson et al. 2014), although Taquet et al. (2013) do not exclude high HDO/H_2O ratios for these same sources. Such a low ratio cannot be reproduced by the chemical predictions except maybe if the ices are built during a translucent phase where the A_V is smaller than 3 or if water is mostly formed when the o/p ratio of H_2 is high Bergin et al. (1999); Taquet et al. (2013). Very high spatial resolution observations of additional HDO and $H_2^{18}O$ lines would then be helpful to firmly confirm that the HDO/H_2O ratio is about 10^{-3} in the most inner regions.

The chaotic profiles of the predicted abundances in the outer regions (see Fig. 2) are difficult to compare with the observations, since the observed abundances have been determined using a simple jump model, in which the envelope is divided in two regions: an inner and an outer regions with both constant abundances with a smaller one in the outer region (Coutens et al. 2012, 2013). Note that the outer region in these jump models includes the two ones that we have defined for radii larger than 70 AU in our model. Regarding the abundance ratios (see Fig.3), the model strongly overproduces the HDO/H_2O ratio. No conclusion can be drawn from the two other abundance ratios since only upper limits on the observed abundance of D_2O have been obtained but the limits are in agreement with our model. If a part of the absorbing layer mentioned in Coutens et al. (2012) is produced in the outermost regions of the envelope, the observed HDO/H_2O ratio could be slightly higher ($\leqslant$ 5%) at the highest radii but it would not reach the 10% predicted by the chemical model and it would not explain the high ratios between $\sim$ 100 and $\sim$ 1000 AU anyway. We conclude this subsection by emphasizing that a proper quantitative comparison of the model predictions with the observations would require the comparison between predicted and observed molecular lines. This way, we would avoid many steps in between the comparison method and inconsistencies between assumptions. Such a methodology would however require the development of a number of comparison tools, which will be done in the future.

2.4 Sensitivity to the parameters

The model results presented in the previous section are not sensitive to the age of the parent cloud (P1).

The modeling results using a C/O elemental ratio of 1.2 (P2) are shown in Fig. 4. Decreasing the oxygen elemental abundance has a strongest effect on the predicted gas-phase abundance of HDO in the inner region of the envelope, decreasing its abundance by more than a factor of 9, whereas H_2O is decreased by a factor of about 6 and D_2O a factor of 5. As a consequence, the HDO/H_2O ratio is slightly increased whereas the other abundance ratios (D_2O/HDO and D_2O/H_2O) are decreased. The impact on the abundance ratios is however small: HDO/H_2O decreases from 0.029 to **0.020**, D_2O/HDO increases from 0.010 to 0.018 and D_2O/H_2O from 3.1×10^{-4} to 3.9×10^{-4}. The main effect of changing the C/O elemental ratio is to decrease the abundance of oxygen available to form those species. The non-linearity of the system makes that the impact on the different species is not the same. In the rest of the envelope, although the change in the abundances is not very strong, it has an impact on the abundance ratios since for radii larger than 200 AU, the H_2O abundance is decreased whereas the D_2O abundance is increased and the HDO abundance is almost unchanged. As a consequence, all abundance ratios (HDO/H_2O, D_2O/HDO and D_2O/H_2O) are increased. The increase of D_2O abundance at this radius when the oxygen elemental abundance is smaller is a surprising result. This behavior is due to the increase of the HDCO abundance in the ices, which is a precursor of D_2O while evaporated in the gas-phase at this radius (see section 2.2). The HDCO molecule is formed on the grains by the dissociation of deuterated methanol CH_2DOH, which is increased by a larger C/O elemental ratio since more carbon is available to form precursors. The HDO/H_2O abundance ratio observed by Coutens et al. (2013) in the center is still reproduced by the model but the D_2O/HDO and D_2O/H_2O predicted ratios get larger than the observed upper limits. In the outer region, the abundance ratios also show a worse agreement with the observations using a 1.2 elemental C/O ratio, except for D_2O/HDO.

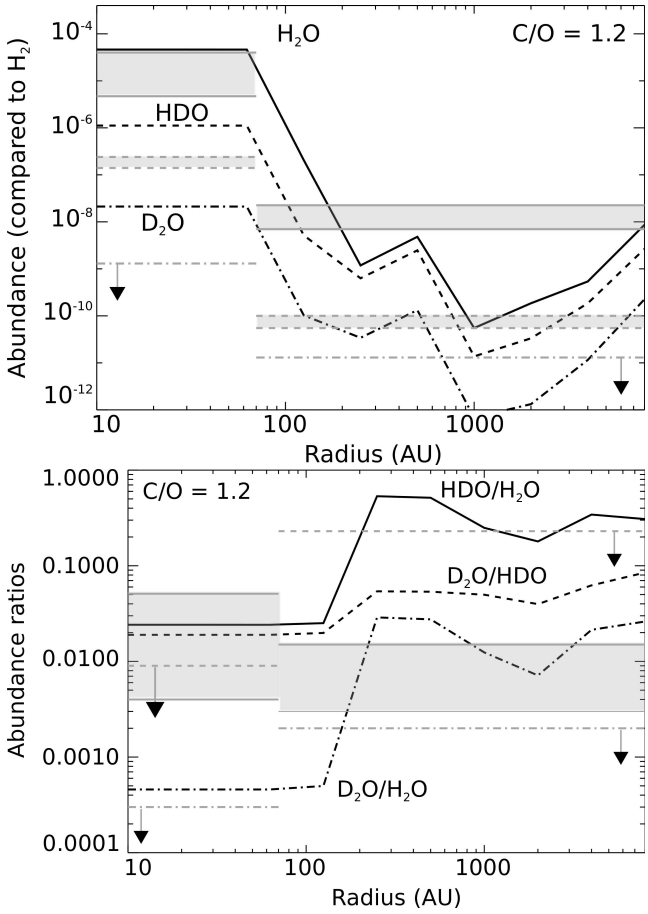

Figure 4. Same as Figs. 2 and 3 but with a C/O elemental ratio of 1.2.

Figure 5 shows the modeling results when the standard model is run with a cosmic-ray ionization rate of 10^{-16} s^{-1} (P3). Abundances of HDO and D_2O in the inner regions are slightly decreased (H_2O stays constant) whereas all three molecules are strongly increased for radius larger than approximately 100 AU. In the inner region, the gas-phase abundances reflects the ice composition. A larger ζ produces more dissociations of HDO and D_2O at the surface of the grains, producing smaller gas-phase abundances while the ices evaporate. In the colder parts of the protostellar envelope, the increase of the three molecules is produced by the increase of the OH and OD abundances (which react with H_2CO and HDCO evaporated from the grains). The increase of those species is due to the dissociation of CH_3OH and CH_2DOH by cosmic-ray induced UV photons. **For the deuterated network used in those simulations, we do not discriminate the isomers of deuterated CH_3OH so that the products of the photodissociation of CH_2DOH and CH_3OD are the same with statistical branching ratios. Since CH_3OD is much less abundant than CH_2DOH, we found that OD is mostly produced by the photodissociation of CH_2DOH.**

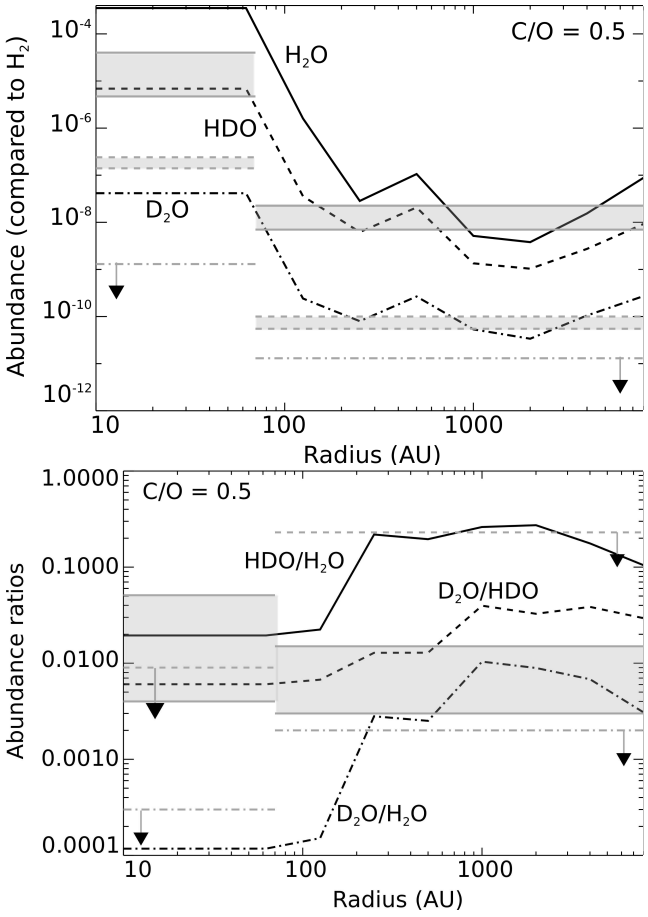

Figure 5. Same as Figs. 2 and 3 but with a cosmic-ray ionization rate of 10^{-16} s^{-1}.

3 THE FOREGROUND CLOUD

3.1 Chemical and physical model description

To study the chemistry of the foreground cloud, called "photodesorption layer" in Coutens et al. (2012, 2013), several models were performed and photo evaporation processes have been added to the model. For this work, a grid of models was performed for the following parameters: temperatures (gas and dust) of 15 and 30 K, total H densities of 2×10^4 and 2×10^5 cm^{-3}, visual extinctions A_V of 2, 3 and 4, cosmic-ray ionization rates of 10^{-17} and 10^{-16} s^{-1}, and C/O elemental ratios of 0.5 and 1.2 (see section 2.1.4). This grid was defined based on the few observational constraints from Coutens et al. (2012). Species are initially in the atomic form with the same elemental abundances as for the protostellar envelope (see section 2.1.4). The photo-evaporation processes of ices by direct and indirect UV photons have been included following the formalism from Visser et al. (2011). For that we have used the same yields of photo-evaporation for deuterated and non-deuterated species as suggested by Öberg et al. (2009a). Experimental results from Öberg et al. (2009a) and Öberg et al. (2009b) have found yields of photo-evaporation about 10^{-3} molecules per grain per incident UV photon, except for N_2. They also showed that this yield may depend on the temperature and the thickness of the ices. We have included the temperature dependence as suggested by the authors but we will show that the efficiency of this process against exothermicity of surface reactions is small under the conditions we have used. All the parameters, which impact on the model predictions have been studied, are summarized in Table 2.

3.2 Gas-phase and ice composition

The first parameter we can exclude is a temperature larger than 15 K. For a temperature of 30 K, the singly and doubly deuterated water abundances are strongly underestimated by the model at all times. Similarly, a visual extinction smaller than 3 produces small amounts of D_2O, much below the observed ones. We then show in Figs. 6, 7, A1 and A2 the modeling results (in the gas and in the ices) for a temperature of 15 K, A_V of 3 and 4, C/O ratios of 0.5 and 1.2, and cosmic-ray ionization rates of 10^{-17} and 10^{-16} s^{-1}. The gas-phase and ice predicted abundances are more sensitive to the parameters when the carbon abundance is larger than the oxygen one so that H_2O and CO are oxygen reservoir competitors. When the C/O elemental ratio is smaller than one, water is the reservoir of oxygen whereas, when C/O is larger than 1 most of the oxygen is stored in CO.

In the cases C/O = 1.2 and A_V smaller than 4, the photodissociations in the gas-phase and at the surface of the grains break the H_2O molecules so that the abundance of this species (and its deuterated forms) is small and most of the oxygen ends up in the gas-phase and icy carbon monoxide CO. When the A_V is large, more H_2O, HDO and D_2O can be formed and remain abundant in the gas-phase. Note that for all three molecules and all models, the abundances on the grain surfaces are larger than the ones in the gas-phase, except in the case of $A_V = 3$ and $\zeta = 10^{-17}$ s^{-1}.

The larger abundances of water obtained for a ζ of 10^{-16} s^{-1} are due to more efficient ion-molecule reaction path than with $\zeta = 10^{-17}$ s^{-1}, which then deplete on the grains. The HDO and D_2O abundances are decreased by the higher ζ on the grains and increased in the gas-phase, except in the case $A_V = 3$. The deuterated water HDO on grains is mainly formed by the surface reactions H_{ice} + OD_{ice} and D_{ice} + OH_{ice}, and the sticking of gas-phase HDO onto the surfaces, whereas it is destroyed by photo-dissociations with direct UV photons and UV photons induced by H_2/cosmic-ray interactions. The larger cosmic-ray ionization rate does not increase the production of HDO on the surface but speeds up strongly its dissociation. In addition, since H atoms are more abundant than D atoms on the surfaces, the photodissociation of HDO → OH + D is more likely followed by the surface reaction OH + H. In the gas-phase, HDO is formed by the dissociative recombination of H_2DO^+, which abundance is increased by the larger ζ. The gas-phase HDO is mostly removed by sticking onto the grain surfaces. Similar conclusions can be drawn for D_2O.

In the case of the smaller C/O ratio (0.5), the predicted abundances are less sensitive to the parameters. This is particularly true for the ice abundances, except for the case of a larger ζ, for which the H_2O_{ice} abundance is increased, and the HDO_{ice} and D_2O_{ice} abundances are decreased. It is interesting to notice that the late time decrease of the gas-phase abundances with the A_V is not as significant as in the case of C/O = 1.2. In the case of an oxygen elemental abundance larger than the carbon one, there is always enough oxygen to reform these molecules even when the photodissociations are efficient.

3.3 Abundance ratios and comparison with the observations

The difficulty to compare those models with the observations comes from the small constraints on the physical structure of the

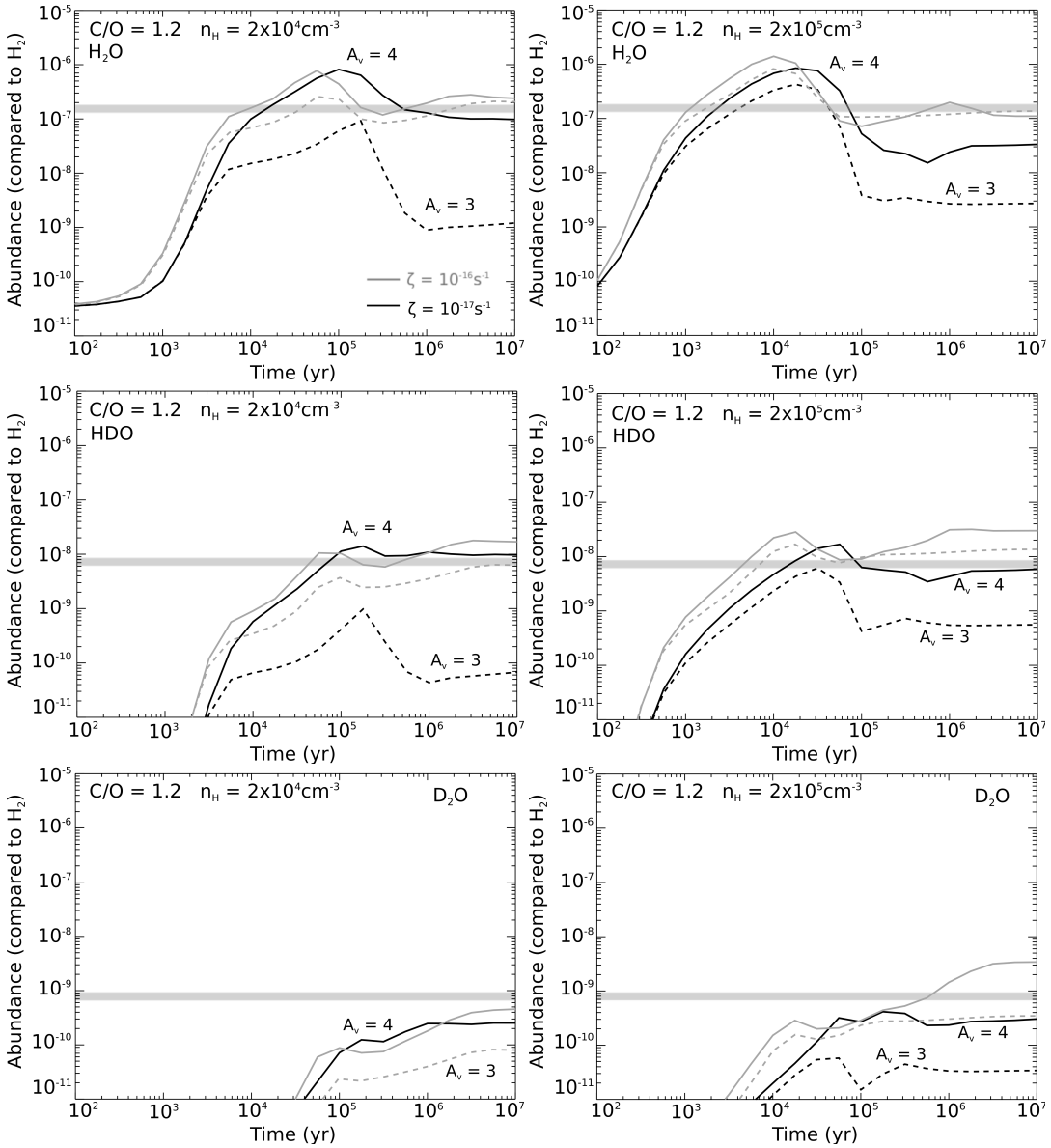

Figure 6. Gas-phase abundances of H_2O, HDO and D_2O as a function of time predicted by the model for the foreground cloud. Gas and dust temperature is the same for all models: 15 K. The elemental C/O abundance ratio is 1.2. The left side of the model has been obtained for a total H density of 2×10^4 cm^{-3} and the right side for a total H density of 2×10^5 cm^{-3}. Black curves have been obtained for a cosmic-ray ionization rate ζ of 10^{-17} s^{-1} whereas grey curves have been obtained for a ζ of 10^{-16} s^{-1}. Solid lines represent an A_V of 4 and dashed lines an A_V of 3. Horizontal grey areas represent the observed values in the foreground cloud for A_V between 3 and 4 (see Table).

source and so the large number of free parameters in our model. The observed abundances in the foreground cloud have been superimposed on Figs. 6 and 7 to the model results. D_2O gives the strongest constraints on the model. For a C/O ratio of 1.2 and if we consider a factor of 2 uncertainty in the observed abundances, only the model with a visual extinction of 4 and a ζ of 10^{-16} s^{-1} can reproduce the observations at late times ($> 3 \times 10^6$ yr) for a density of 2×10^4 cm^{-3} and between 2×10^5 and 10^6 yr for a larger density of 2×10^5 cm^{-3}. Under those conditions, the observed abundances of HDO and H_2O are also reproduced. Using the C/O elemental ratio of 0.5, less constraints can be brought on the other parameters. D_2O for instance is sufficiently produced whatever A_V and ζ for a density of 2×10^5 cm^{-3}. For a ten times less dense cloud, a large A_V of 4 is required. From a general point of view, the constraints set by the HDO and D_2O abundances are small in that case. The predicted gas-phase abundance ratios HDO/H_2O, D_2O/HDO and D_2O/H_2O as a function of time are shown in Figs. 9 and 8 with the observational constraints. Whatever the C/O elemental ratio, the models with the smallest density (2×10^4 cm^{-3}) seem to underestimate the D_2O/HDO and D_2O/H_2O ratios.

To compare the models to the observations in a more quantitative way, we have used the method introduced in Loison et al. (2014). For the three molecules, we have compared the observed and modeled abundances by calculating the mean distance of disagreement as a function of time : $\Sigma|\log(X_i) - \log(X_{i,obs})|/3$, with X_i the abundance of species i (H_2O, HDO or D_2O) computed by the model and $X_{i,obs}$ the observed abundance. Such calculation has been done for all models and the results are shown in Fig. 10. Con-

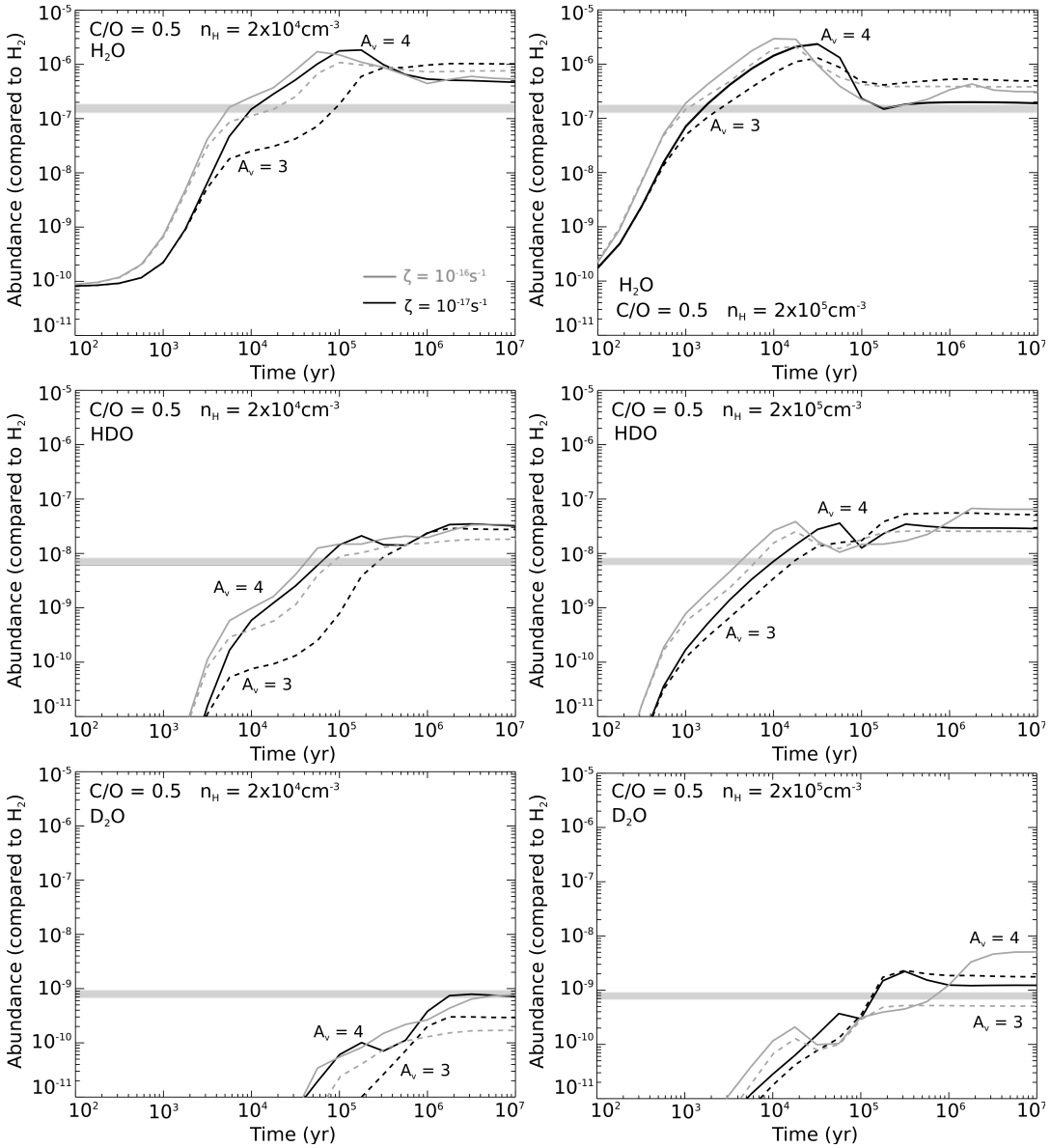

Figure 7. Same as Fig. 7 but a C/O of 0.5.

sidering the models with a C/O elemental ratio of 0.5, the higher density (2×10^5 cm^{-3}) gives the best agreement whatever the A_V and ζ. For these later cases, the mean distance of disagreement is between 0.2 and 0.3 (in log), which means that the observed and modeled abundances show a difference between a factor of 1.6 and 2 in average. For a larger C/O ratio, only the case with a large ζ and A_V gives a satisfactory agreement for times equal to or larger than 10^6 yr.

4 DISCUSSION

4.1 Effect of the photo-evaporation

In the simulations that we have done for the protostellar outer envelope and the foreground cloud, the abundances of water and its deuterated forms are larger on the grain surfaces than in the gas-phase by several orders of magnitude in many cases. Without any non-thermal evaporation processes of the icy grain mantles, the predicted gas-phase abundances of these species would be much smaller. Hollenbach et al. (2009) found that using their model, they would produce large abundances of gas-phase water, similar to ours, at the border of dense clouds by photo-evaporation of the ices at A_V between 3 and 8. Although we have included photo-evaporation of grain mantles by direct and indirect UV photons, it is not this process that drives the evaporation of the mantles and produce large gas-phase H_2O abundances. In our case, the exothermicity of the surface reactions, that allow for partial evaporation of the products, releases H_2O, HDO and D_2O into the gas-phase by the following reactions:

$$H_{ice} + OH_{ice} \rightarrow H_2O_{gas}, \quad (9)$$

$$H_{ice} + OD_{ice} \rightarrow HDO_{gas}, \quad (10)$$

$$D_{ice} + OH_{ice} \rightarrow HDO_{gas}, \quad (11)$$

$$D_{gas} + OD_{ice} \rightarrow D_2O_{gas}. \quad (12)$$

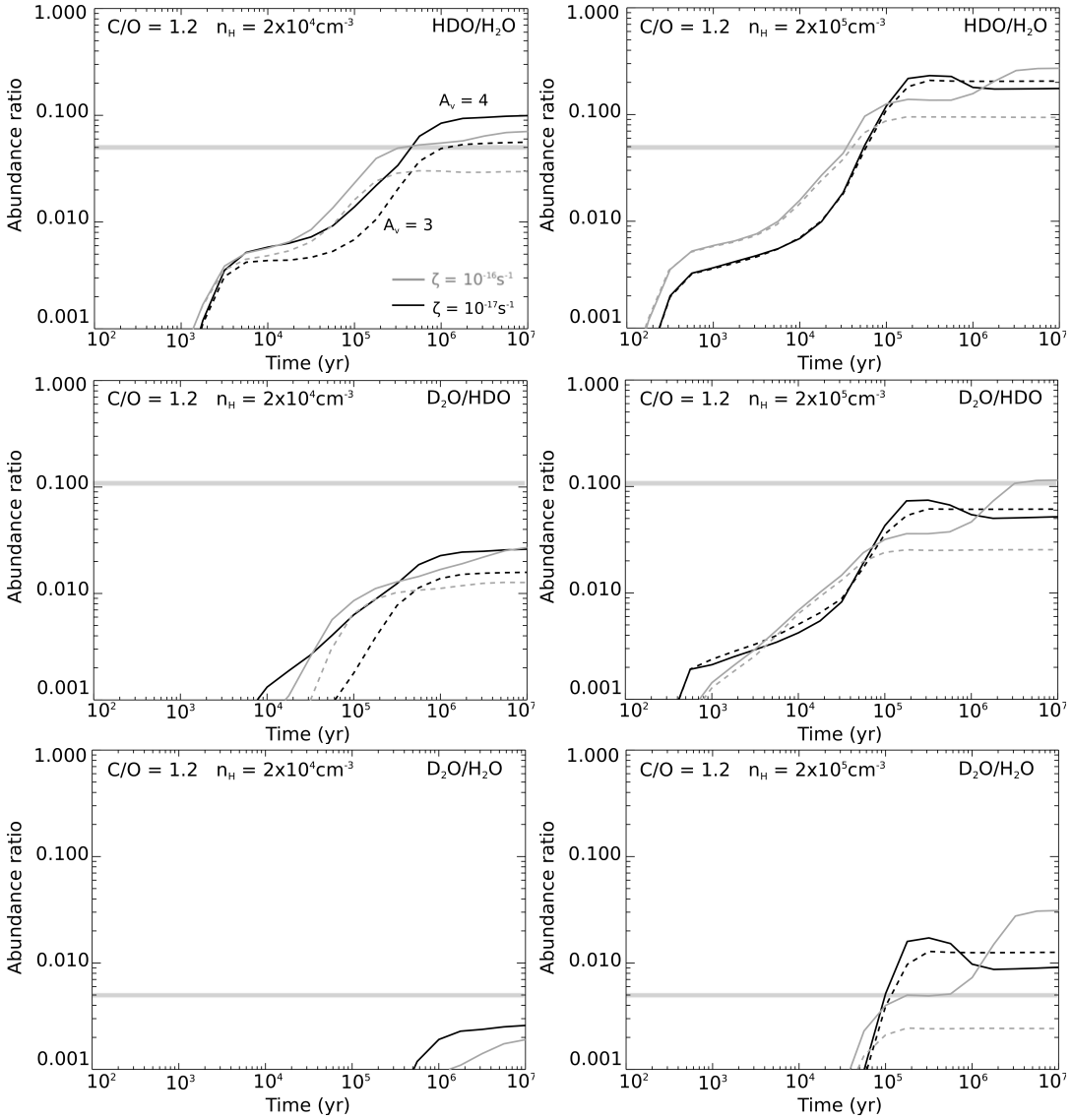
C/O = 1.2 n_H = 2x10^4cm^-3 HDO/H2O
C/O = 1.2 n_H = 2x10^5cm^-3 HDO/H2O
C/O = 1.2 n_H = 2x10^4cm^-3 D2O/HDO
C/O = 1.2 n_H = 2x10^5cm^-3 D2O/HDO
C/O = 1.2 n_H = 2x10^4cm^-3 D2O/H2O
C/O = 1.2 n_H = 2x10^5cm^-3 D2O/H2O
A_v = 4
A_v = 3
ζ = 10^-16 s^-1
ζ = 10^-17 s^-1
Abundance ratio
Time (yr)

Figure 8. Same as Fig. 9 but a C/O of 1.2.

Removing this process decreases the gas-phase abundances of water and deuterated water by a factor of 10 in some cases. Following Garrod et al. (2007), the fraction of products allowed to evaporate is 0.7%. This value is, however, far from being constrained. Previous experiments from Kroes & Andersson (2006) have set a 1% limit for the efficiency of this process whereas Dulieu et al. (2013) have recently found that the chemi-desorption could be more efficient in particular during the formation of water. Increasing the fraction of desorption in our model would increase the abundances of these molecules in the gas-phase.

The direct photo-evaporation of icy mantles by UV photons depends on the intensity of the UV irradiation field but does not increase linearly with it. Although the rate of photo-evaporation is proportional to the intensity of the UV field, the rate is also multiplied by a dimensionless factor that indirectly depends on the UV field: $f(X) = n_s(X)/n_{ice}$ where $n_s(X)$ is the number density of species X in the ices and n_{ice} is the total number density of all ice species. This factor aims at taking into account the 0 order behavior of this reaction when more than one monolayer of molecules is present on the surfaces (see Visser et al. 2011). When the intensity of the UV field is changed, the number of species on the surfaces is also changed. All simulations presented in this paper have been obtained for a standard interstellar UV field (1 G_0). For an A_V of 4, if the UV field is 10 times larger, the HDO and D_2O abundances are decreased due to more photodissociations. Even in that case, the photo-evaporation processes remain unimportant compared to the exothermicity of the surface reactions, i.e. models with and without photo evaporation will produce the same results.

4.2 Effect of C/O and cosmic-ray ionization rate on D/H

To look at the effect of the C/O elemental ratio and the cosmic-ray ionization rate on the D/H ratio measured in deuterated water, we show in Fig. 11 the following abundance ratio $(0.5X_{HDO} + X_{D_2O})/X_{H_2O}$ as a function of time for two densities (2×10^4 and 2×10^5 cm^{-3}), two C/O elemental ratios (C/O = 0.5 and 1.2) and two cosmic-ray ionization rates (10^{-17} and 10^{-16} s^{-1}). The temperature is 15 K and the A_V is 4. We present the D/H ratio predicted 1) in

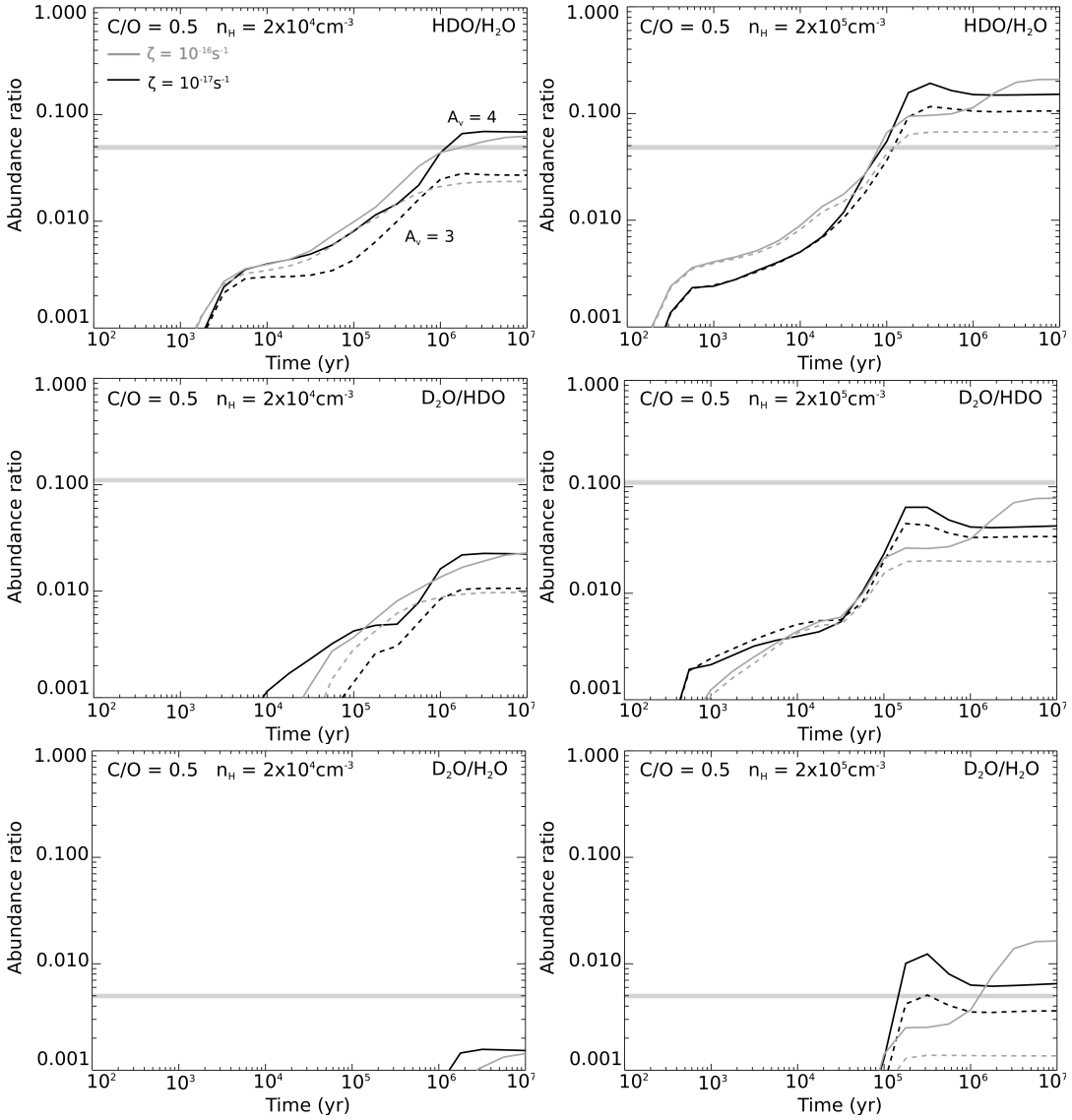

Figure 9. Gas-phase abundance ratios HDO/H_2O, D_2O/HDO and D_2O/H_2O as a function of time predicted by the model for the foreground cloud. Gas and dust temperature is the same for all models: 15 K. The elemental C/O abundance ratio is 0.5. The left side of the model has been obtained for a total H density of 2×10^4 cm^{-3} and the right side for a total H density of 2×10^5 cm^{-3}. Black curves have been obtained for a cosmic-ray ionization rate ζ of 10^{-17} s^{-1} whereas grey curves have been obtained for a ζ of 10^{-16} s^{-1}. Solid lines represent an A_V of 4 and dashed lines an A_V of 3.

the gas-phase only and 2) considering both the gas-phase and grain surface abundances. The D/H ratio increases with time in all cases as the molecules are built up, except for the case of a larger ζ where the species at the surface of the grains are destroyed. Considering only water in the gas-phase, the D/H ratio is less sensitive to the C/O elemental ratio and ζ than to the density of the medium. Larger densities produce larger D/H ratios. Considering the full budget of water (both in the gas-phase and at the surface of the grains), D/H is strongly sensitive to the cosmic-ray ionization rate, even more than to the density. The larger ζ decreases strongly D/H at times larger than 10^5 yr. In general, large C/O seems to produce slightly larger D/H.

4.3 Elemental abundance of deuterium

The deuterium elemental abundance is set to 1.5×10^{-5} compared to H, which is the average value found by absorption spectroscopy measurements towards stars in the vicinity of the Sun (e.g. Linsky et al. 2006). Linsky et al. (2006) argued that these measurements inside the so-called "Local Bubble" may not be representative of the deuterium abundance in the galactic disk beyond. Indeed, spatial variations in the depletion of deuterium from the gas phase onto dust grains (Jura 1982; Draine 2004, 2006) can explain these local variations in the observed gas-phase D/ H ratios. In our standard model, we used the value of 1.5×10^{-5} and envision the influence of its uncertainty on our modeling.

When the deuterium elemental abundance is multiplied or divided by a factor of two compared to its nominal value given in section 2.1.4, the HDO gas-phase and ice abundances are also multiplied and divided but by less than a factor of two. Similarly, D_2O is modified by less than a factor of four. The abundance ratios are also modified by an amount depending on the model but, from a general point of view, an increase of D elemental abundance increases the three ratios HDO/H_2O, D_2O/HDO and D_2O/H_2O.

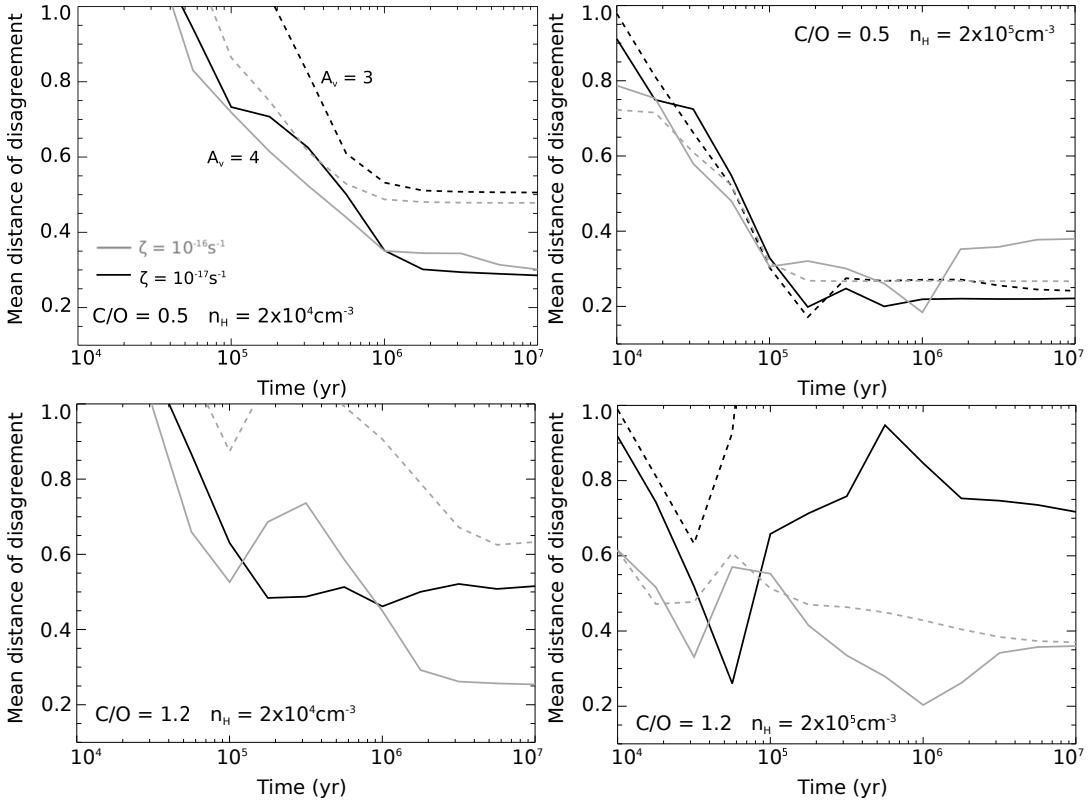
Mean distance of disagreement
Time (yr)
A$_v$ = 3
A$_v$ = 4
ζ = 10^{-16}s^{-1}
ζ = 10^{-17}s^{-1}
C/O = 0.5 n$_H$ = 2x10^{4}cm^{-3}
C/O = 0.5 n$_H$ = 2x10^{5}cm^{-3}
C/O = 1.2 n$_H$ = 2x10^{4}cm^{-3}
C/O = 1.2 n$_H$ = 2x10^{5}cm^{-3}

Figure 10. Mean distance of disagreement as a function of time for the foreground cloud. Gas and dust temperature is the same for all models: 15 K. The elemental C/O abundance ratio is 0.5 for the upper panels and 1.2 for the lower panels. The left side of the model has been obtained for a total H density of 2×10^4 cm^{-3} and the right side for a total H density of 2×10^5 cm^{-3}. Black curves have been obtained for a cosmic-ray ionization rate ζ of 10^{-17} s^{-1} whereas grey curves have been obtained for a ζ of 10^{-16} s^{-1}. Solid lines represent an A_V of 4 and dashed lines an A_V of 3.

4.4 Importance of the ortho/para ratio of H_2 on the formation of deuterated water

As mentioned in the presentation of the deuterated network (section 2.1.2), we did not include the ortho H_2. Ortho and para H_2 will react differently for some reactions. One reaction is of particular importance for the deuteration: $H_2D^+ + H_2 \rightarrow H_3^+ + HD$. Para H_2 in this reaction reacts very slowly compared to ortho H_2. According to Hugo et al. (2009), the difference between the two rate coefficients is more than four orders of magnitude at 10 K. A faster rate coefficient decreases the efficiency of the production of deuterated species. We have tested the effect of considering the higher reactivity of ortho H_2 by replacing the rate coefficient of this reaction by the one from ortho H_2 ($k(T) = 4.67 \times 10^{-11} \exp(0.82/T)$, Hugo et al. 2009)) times the ortho to para H_2 ratio. For the ortho to para H_2 ratio, we have considered three values that are fixed with time and temperature: 10^{-3} which is the value constrained by Dislaire et al. (2012) in the outer envelope of IRAS16293, 0.1 which is the value proposed by several authors in cold dense clouds (Pagani et al. 2011; Caselli et al. 2012), and 3 which is the statistical value of their formation on the grains. In all the simulations that we have done, a o/p H_2 ratio of 10^{-3} does not affect significantly the results presented in the paper. For larger values, it does and we will now discuss the main consequences.

At the low temperatures considered for the foreground cloud, the Boltzmann value of the o/p H_2 ratio is very low (10^{-4}). The grains however are expected to form o-H_2 and p-H_2 in the ratio 3:1 so the main uncertainty should be the time of conversion from 3 to it Boltzmann value. We have shown the results of the tests in Fig. B1. Considering an o/p H_2 ratio of 0.1 and above decreases the predicted abundances of HDO and D_2O in the gas-phase too strongly compared to the observed values listed in Table 1. Using a full gas-grain model including the ortho and para forms of H_2, Taquet et al. (2013) concluded that the o/p H_2 ratio should be small (smaller than 3×10^{-4}) in IRAS16293 to reproduce the deuterated water in the outer parts of this source.

In the protostellar envelope, the gas temperature increases with time as the shells of material move towards the center. Considering fixed o/p H_2 ratios is then a strong approximation but allows us to frame the effect. The modeling results are shown in Fig. B2. Increasing the o/p H_2 ratio decreases the abundances of HDO and D_2O in the gas-phase without changing significantly H_2O in the entire envelope. In the inner hot corino region, the HDO and D_2O abundances get closer to the observational constraints from Coutens et al. (2013) but in that case the abundance ratios HDO/H_2O and D_2O/H_2O are not reproduced anymore. In the case of a fixed o/p H_2 ratio of 0.01, the HDO/H_2O abundance ratio is 2×10^{-3} and for an o/p H_2 ratio of 3, it becomes 5×10^{-4}. In those cases, the HDO/H_2O ratio is in agreement the values observed by Persson et al. (2013). In the intermediate and outer regions of the envelope, the HDO abundance gets closer to the observations but is still over predicted by the model even for an o/p H_2 ratio of 3, as well as the HDO/H_2O ratio. The D_2O/H_2O abundance ratio becomes in agreement with the observations for o/p H_2 larger or equal to 0.01. The HDO/H_2O ratio is still predicted by the model to be larger than D_2O/HDO. To maybe be more realistic, we redid those simulations but assumed an o/p H_2 ratio temperature depen-

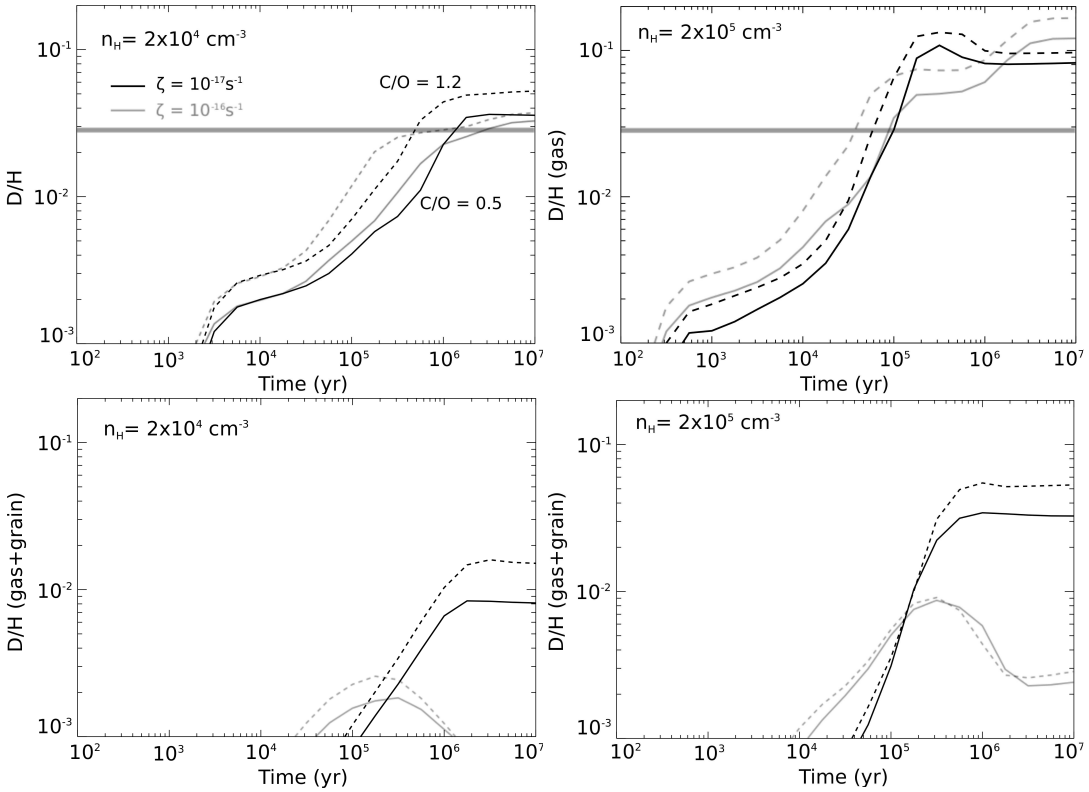

Figure 11. D/H ratio predicted by the model in the gas-phase deuterated water (top row) and considering both the gas-phase and grain surface deuterated water (bottom row). Two densities are considered: 2×10^4 cm^{-3} on the left and 2×10^5 cm^{-3} on the right, two C/O elemental ratios (C/O = 0.5 for the solid curves and C/O = 1.2 for dashed curves) and two cosmic-ray ionization rates (10^{-17} s^{-1} for black curves and 10^{-16} s^{-1} for grey curves). Grey area represents the D/H ratio observed in the foreground cloud.

dent using the relation o/p H_2 ratio = $9\times\exp -170.5/T$ at the Boltzmann equilibrium. **Using this relation, the o/p H_2 ratio increases along with the temperature during the collapse of the protostellar envelope. Considering the shell of material that ends up in the inner region of the envelope (inside 75 AU), the initial o/p H_2 ratio is only 5×10^{-9} (T=8 K) whereas it is above 1.6 at the end of the simulations (T⩽100 K). However, the timescale of the collapse implies that the material stays at low temperature for a much longer period of time than at high temperature (see Aikawa et al. 2008). In fact, as previously mentioned, the deuterated water is formed in the ices at low temperature when the o/p H_2 ratio is low. Then when the temperature increases, HDO and D_2O are evaporated in the gas-phase but not efficiently destroyed. As a consequence the abundance predictions are not changed compared to our nominal model. If the collapse was much faster, with an initial pre-collapse phase shorter than 2×10^5 yr, the formation of deuterated water could be less efficient producing a smaller HDO/H_2O ratio. Further investigation in this direction should however be done to quantitatively conclude on this question.**

4.5 The physical structure of the protostellar envelope

To analyze the observed lines of H_2O, HDO and D_2O in the envelope of IRAS16293, Coutens et al. (2012, 2013) used the physical structure constrained by Crimier et al. (2010) from dust emission at several wavelength (see Fig. 1). These temperature and density profiles are similar to the ones we obtain for a protostellar age of 9×10^4 yr using the RHD model from Masunaga & Inutsuka (2000) except that the densities are approximately ten times larger at a given radius. To be more consistent with the observations, we have thus multiplied the densities at each radius and all along the calculation by a factor of ten. Doing that, the temperatures and timescales of collapse are not consistent anymore.

The RHD model starts with a hydrostatic sphere of 3.852 M⊙ over a radius of 4×10^4 AU. At the final time (9×10^4 yr after the birth of the protostar), the mass of the protostar (inside 4 R⊙) is approximately 1 M⊙ and the luminosity 31 L⊙. The mass accretion rate is constant with time to a value of $\sim 5.3 \times 10^{-6}$ M⊙ yr^{-1}. Crimier et al. (2010) estimated a protostellar mass of 2 M⊙ with a luminosity of 22 L⊙. The mass is then two times larger than in our case whereas the luminosity is smaller. The mass accretion rate was determined by Ceccarelli et al. (2000) to be 3.5×10^{-5} M⊙ yr^{-1}, much larger than in our model. Other numbers for the mass of the protostar have been published in the literature ranging from 0.8 M⊙ (Ceccarelli et al. 2000) to 6.1 M⊙ (Stark et al. 2004). Using ALMA observations of dust and complex molecules, Pineda et al. (2012) derived a mass of 0.21 and 0.26 M⊙ for sources A and B. IRAS1293 is indeed a binary (even maybe triple) system. All observations discussed up to now in this paper are single dish and so do not separate the different sources. The interferometric observations show that the two sources present very different kinematics. B presents clear infall signature whereas A seems to be consistent with a rotating disk. Considering all these uncertainties in the observational constraints of IRAS16293 physical structure, it seems difficult to improve our modeling at this point.

That said, we can discuss the feedback of increasing the densities in our model and the importance of these assumptions for

the chemistry. A denser envelope has two opposite effects on the temperature. Since the core is heated on the inside, the higher density would increase the opacity of the core and then decrease the temperature. On the other hand, a denser and so more massive envelope would mean a larger mass accretion rate, which would produce larger temperatures. To understand the feedback of a denser envelope on the temperature, the RHD model would have to be run again using different parameters. This will be done in the future. Another effect of the denser envelope is to slow down the time of free-fall. To test this effect, we have run our model reducing dynamical time of collapse of all cells by a factor of 3. This does not change significantly the results. In addition, we run our model using the original density profile from the RHD model. This on the contrary modified strongly our results for radius larger than 100 AU. Smaller densities produce less depletion and so the H_2O, HDO and D_2O abundances are larger but not affected the same way. As a consequence, the abundance ratios are very different from the ones shown in this paper. This result points out the crucial need for accurate estimates of the physical conditions in protostellar envelope for chemical studies.

4.6 Comparison with other works

Deuteration in star forming regions have been extensively studied from the observation and modeling points of view. We will compare our results with a few other recent published works on the modeling of deuterated water. Cazaux et al. (2011) studied the formation of deuterated species in ices in translucent clouds evolving towards denser clouds. The model does not include gas-phase chemistry but allows the sticking of gas-phase species onto the surface of the grains and follows the formation of the species at the surface of the grains. The density of the cloud is computed by the equation of free-fall whereas several dust temperatures are considered from 12 K to 17 K. The authors found that the formation of deuterated water on ices strongly depends on the dust temperature within this range: at low temperature the large abundance of H_2 on the surface favors the formation of water whereas at 17 K, H_2 evaporates and produces larger HDO/H_2O ratios. The considered reactions of oxygen with molecular hydrogen are endothermic and in our model, as in Taquet et al. (2013), the formation of water mostly occurs through reactions with atomic hydrogen. As a consequence, we do not expect to find such a strong temperature sensitivity.

Three other deuterated models have recently been published using a gas-grain chemical model similar to ours: Albertsson et al. (2013), Taquet et al. (2013) and Sipilä et al. (2013). Albertsson et al. (2013) studied the deuteration in a large range of temperatures and density but for a fixed visual extinction (of 10), cosmic-ray ionization rate (of 10^{-17} s^{-1}) and evolution time (of 1 Myr). Similarly to Aikawa et al. (2012), they extended a large gas-grain network to include the deuteration, without considering the ortho form of H_2. The main point of this work is to identify the key reactions for the deuteration in the various conditions. For physical conditions similar to hot corinos, they found an abundance ratio between 10^{-3} and 10^{-2} (see their Table 19), which is smaller compared to our predictions. The difference is very likely due to the different physical conditions used in both models. Taquet et al. (2013) did also a parameter space study of the deuteration of water using a two phase model (a chemically inactive bulk and a surface layer). Their main conclusion is that the HDO/H_2O and D_2O/H_2O abundance ratios are highly dependent in the density and the visual extinction (between 2 and 5) of the medium. We do find similar results. To quantitatively compared their results to ours, we have used the foreground model for a visual extinction of 4, a temperature of 15 K, a cosmic-ray ionization rate of 1.3×10^{-17} s^{-1}, a C/O ratio of 0.5 and a density of 2×10^5 cm^{-3} and compared with the Fig. 8 from Taquet et al. (for a temperature of 10 K and a density of 10^5 cm^{-3}). The HDO/H_2O and D_2O/H_2O abundance ratios in the ices of our model presents the same shape as a function of time and reaches a steady-state value at approximately the same age. In our case, the maximum HDO/H_2O value is 0.065 and the one of D_2O/H_2O is 10^{-3}. Those values agree quite well with the ones predicted by Taquet et al. We do also predict that the abundance ratios **increase** with the density. The same comparison can be made with the Fig. 11 from Sipilä et al. (2013). Despite the fact that they do not reach a steady-state value, we obtain HDO/H_2O abundance ratios in the ices that are similar at 10^7 yr. In their model, Sipilä et al. (2013) considered ortho and para forms of H_2 and a time dependent o/p ratio. This may explain the differences.

5 CONCLUSIONS

In this paper, we have done a modeling of the chemistry towards the protostellar envelope of the low-mass protostar IRAS16293-2422 using a gas-grain chemical model (Nautilus), a deuterated gas-grain network and a dynamical model of the protostellar collapse. The model has been used to reproduce the observations of H_2O, HDO and D_2O towards this source using ground based telescopes and the HIFI spectrometer on board the Herschel telescope observed by Coutens et al. (2012, 2013). Part of the emission of molecules was identified to come from a foreground cloud in addition to the protostellar envelope. Using a multi-parameter study of the chemistry, we try to put some constraints on the physical parameters of this foreground cloud as well as the protostellar envelope. The following conclusions can be drawn.
For the central part of the protostellar envelope:

- In a 1D model, the abundance ratios HDO/H_2O, D_2O/HDO and D_2O/H_2O are predicted to be constant in the inner 100 AU even though the full evaporation of the mantle ices only occurs for radii smaller than 60 AU.
- The H_2O, HDO and D_2O observed abundances are strongly overproduced by the model in the inner region of the protostellar envelope. The reason may be the presence of a more complex structure within the inner 100 AU. Future investigations with 2D or 3D physical structure, both for the analysis of the observations and the chemical model will be needed.
- The observed abundance ratios HDO/H_2O, D_2O/HDO and D_2O/H_2O are better reproduced by the model using a cosmic-ray ionization rate of 10^{-16} s^{-1} and a C/O elemental ratio of 0.5.

For the outer part of the protostellar envelope:

- The observed abundances of H_2O, HDO and D_2O and abundance ratios HDO/H_2O, D_2O/HDO and D_2O/H_2O are not well reproduced by our model in the outer part of the protostellar envelope whatever the parameters used. Abundance ratios are systematically overproduced by the models. One has to note the difference between the chaotic abundance profiles profiles predicted by the model, which are very different from the jump model used for the analysis of the observations. In addition, it is possible that part of the emission that was attributed to the foreground cloud indeed come from the outer part of the envelope. In this case, the observed abundances and D/H ratios could be larger than the ones used for this comparison.

- Both for the inner and outer regions of the protostellar envelope, the age of the cloud prior collapse does not seem to play a major role for the H_2O, HDO and D_2O abundances.

For the foreground cloud:

- To reproduce the observation of water and deuterated water in this foreground cloud, the temperature needs to be small (about 15 K) and the visual extinction larger or equal to 3. Within these limits, several C/O ratios and cosmic-ray ionization rates can reproduce the observations at a satisfactory level. If the C/O ratio is 0.5, the cloud density may be large (of about 2×10^5 cm^{-3}) whereas if the C/O ratio is 1.2, the observations constrain the cosmic-ray ionization rate to be large (of about 10^{-16} s^{-1}).

- As for the CH modeling from Bottinelli et al. (2014), the larger densities shows a better agreement for earlier times. The "best" times are however not consistent with the present constraints and are ten times larger for deuterated water. For a density of 2×10^5 cm^{-3} for instance, CH observed abundances were reproduced around 10^4 yr whereas H_2O, HDO and D_2O are reproduced around 2×10^5 yr in the present study. Better constraints on the physical properties of this foreground cloud are clearly needed. This could be achieved by studying other molecules that could trace this layer of gas using the same method.

- This foreground cloud was baptized "photodesorption layer" by Coutens et al. (2013) arguing that considering the small A_V the photo-evaporation of ices may control the gas-phase abundances of these species. We have shown that, in our model, it is the exothermicity of the reactions at the surface of the grains that would release H_2O, HDO and D_2O during their formation at the surface rather than the photo-evaporation.

- Although some of our models show a good agreement with the observations, the model always found a D_2O/HDO abundance ratio smaller than the HDO/H_2O one, contrary to the observations. Indeed, the observations suggest that the conversion of HDO into D_2O is more efficient than the conversion of H_2O into HDO or that D_2O would be more efficiently evaporated than HDO.

Finally, we have neglected the importance of the ortho form of H_2 in this model. Further works are needed to check its importance for the formation of water and deuterated water under the conditions considered for the different layers in the line of sight of IRAS16293.

ACKNOWLEDGMENTS

VW thanks the following funding agencies for their partial support of this work: the French CNRS/INSU program PCMI and the ERC Starting Grant (3DICE, grant agreement 336474). VW is grateful to Prof. Eric Herbst, George Hassel and Franck Hersant for fruitful discussions on photo-evaporation processes. We would like to thank the referee for providing useful comments that helped us improve the content of the paper.

REFERENCES

Aikawa Y., Kamuro D., Sakon I., Itoh Y., Terada H., Noble J. A., Pontoppidan K. M., Fraser H. J., Tamura M., Kandori R., Kawamura A., Ueno M., 2012, A&A, 538, A57

Aikawa Y., Wakelam V., Garrod R. T., Herbst E., 2008, ApJ, 674, 984

Aikawa Y., Wakelam V., Hersant F., Garrod R. T., Herbst E., 2012, ApJ, 760, 40

Albertsson T., Semenov D. A., Vasyunin A. I., Henning T., Herbst E., 2013, ApJS, 207, 27

Andersson S., Al-Halabi A., Kroes G.-J., van Dishoeck E. F., 2006, J. Chem. Phys., 124, 064715

Andersson S., van Dishoeck E. F., 2008, A&A, 491, 907

Atkinson R., Baulch D. L., Cox R. A., Crowley J. N., Hampson R. F., Hynes R. G., Jenkin M. E., Rossi M. J., Troe J., 2004, Atmospheric Chemistry & Physics, 4, 1461

Bergin E. A., Neufeld D. A., Melnick G. J., 1999, ApJ, 510, L145

Bockelée-Morvan D., Biver N., Swinyard B., de Val-Borro M., Crovisier J., Hartogh P., Lis D. C., Moreno R., Szutowicz S., Lellouch E., Emprechtinger M., Blake G. A., Courtin R. e. a., 2012, A&A, 544, L15

Bottinelli S., Wakelam V., Caux E., Vastel C., Aikawa Y., Ceccarelli C., 2014, MNRAS, 441, 1964

Butner H. M., Charnley S. B., 1997, in American Astronomical Society Meeting Abstracts Vol. 29 of Bulletin of the American Astronomical Society, Detection of Alfven Waves by Molecular Spectroscopy - Deuterium Chemistry. p. 1245

Caselli P., Keto E., Bergin E. A., Tafalla M., Aikawa Y., Douglas T., Pagani L., Yíldíz U. A., van der Tak F. F. S., Walmsley C. M., Codella C., Nisini B., Kristensen L. E., van Dishoeck E. F., 2012, ApJ, 759, L37

Caselli P., Walmsley C. M., Terzieva R., Herbst E., 1998, ApJ, 499, 234

Cazaux S., Caselli P., Spaans M., 2011, ApJ, 741, L34

Ceccarelli C., Castets A., Caux E., Hollenbach D., Loinard L., Molinari S., Tielens A. G. G. M., 2000, A&A, 355, 1129

Charnley S. B., 1997, ApJ, 481, 396

Coutens A., Vastel C., Cabrit S., Codella C., Kristensen L. E., Ceccarelli C., van Dishoeck E. F. e. a., 2013, A&A, 560, A39

Coutens A., Vastel C., Caux E., Ceccarelli C., Bottinelli S., Wiesenfeld L., Faure A., Scribano Y., Kahane C., 2012, A&A, 539, A132

Coutens A., Vastel C., Cazaux S., Bottinelli S., Caux E., Ceccarelli C., Demyk K., Taquet V., Wakelam V., 2013, A&A, 553, A75

Crimier N., Ceccarelli C., Maret S., Bottinelli S., Caux E., Kahane C., Lis D. C., Olofsson J., 2010, A&A, 519, A65

Cuppen H. M., Ioppolo S., Romanzin C., Linnartz H., 2010, Physical Chemistry Chemical Physics (Incorporating Faraday Transactions), 12, 12077

Dartois E., Thi W.-F., Geballe T. R., Deboffle D., d'Hendecourt L., van Dishoeck E., 2003, A&A, 399, 1009

de Graauw T., Helmich F. P., Phillips T. G., Stutzki J., Caux E., Whyborn N. D., Dieleman P., Roelfsema P. R., Aarts H., Assendorp R., Bachiller R., Baechtold W., Barcia A., Beintema D. A., Belitsky V., Benz A. O., et al. 2010, A&A, 518, L6

Dislaire V., Hily-Blant P., Faure A., Maret S., Bacmann A., Pineau Des Forêts G., 2012, A&A, 537, A20

Doty S. D., Schöier F. L., van Dishoeck E. F., 2004, A&A, 418, 1021

Dulieu F., Amiaud L., Congiu E., Fillion J.-H., Matar E., Momeni A., Pirronello V., Lemaire J. L., 2010, A&A, 512, A30

Dulieu F., Congiu E., Noble J., Baouche S., Chaabouni H., Moudens A., Minissale M., Cazaux S., 2013, Scientific Reports, 3

Dutrey A., Wakelam V., Boehler Y., Guilloteau S., Hersant F., Semenov D., Chapillon E., Henning T., Piétu V., Launhardt R., Gueth F., Schreyer K., 2011, A&A, 535, A104

Fraser H. J., Collings M. P., McCoustra M. R. S., Williams D. A., 2001, MNRAS, 327, 1165
Garrod R. T., Herbst E., 2006, A&A, 457, 927
Garrod R. T., Wakelam V., Herbst E., 2007, A&A, 467, 1103
Hartogh P., Lis D. C., Bockelée-Morvan D., de Val-Borro M., Biver N., Küppers M., Emprechtinger M., Bergin E. A., Crovisier J., Rengel M., Moreno R., Szutowicz S., Blake G. A., 2011, Nature, 478, 218
Hartquist T., 2003, Astronomy and Geophysics, 44, 020000
Hasegawa T. I., Herbst E., 1993, MNRAS, 261, 83
Hasegawa T. I., Herbst E., Leung C. M., 1992, ApJS, 82, 167
Hily-Blant P., Maret S., Bacmann A., Bottinelli S., Parise B., Caux E., Faure A., Bergin E. A., Blake G. A., Castets A., Ceccarelli C., Cernicharo J., Coutens A., Crimier N., Demyk K. e. a., 2010, A&A, 521, L52
Hincelin U., Wakelam V., Hersant F., Guilloteau S., Loison J. C., Honvault P., Troe J., 2011, A&A, 530, A61
Hirota T., Ikeda M., Yamamoto S., 2001, ApJ, 547, 814
Hogerheijde M. R., Bergin E. A., Brinch C., Cleeves L. I., Fogel J. K. J., Blake G. A., Dominik C., Lis D. C., Melnick G., Neufeld D., Panić O., Pearson J. C., Kristensen L., Yıldız U. A., van Dishoeck E. F., 2011, Science, 334, 338
Hogerheijde M. R., van der Tak F. F. S., 2000, A&A, 362, 697
Hollenbach D., Kaufman M. J., Bergin E. A., Melnick G. J., 2009, ApJ, 690, 1497
Hugo E., Asvany O., Schlemmer S., 2009, J. Chem. Phys., 130, 164302
Indriolo N., McCall B. J., 2012, ApJ, 745, 91
Ioppolo S., Cuppen H. M., Romanzin C., van Dishoeck E. F., Linnartz H., 2010, Physical Chemistry Chemical Physics (Incorporating Faraday Transactions), 12, 12065
Jørgensen J. K., van Dishoeck E. F., 2010a, ApJ, 725, L172
Jørgensen J. K., van Dishoeck E. F., 2010b, ApJ, 710, L72
Kristensen L. E., van Dishoeck E. F., Bergin E. A., Visser R., Yıldız U. A., San Jose-Garcia I., Jørgensen J. K., Herczeg G. J., Johnstone D., Wampfler S. F., Benz A. O., Bruderer S., Cabrit S. e. a., 2012, A&A, 542, A8
Kroes G. J., Andersson S., 2006, IAU Symp., 231, 427
Leger A., Jura M., Omont A., 1985, A&A, 144, 147
Linsky J. L., Draine B. T., Moos H. W., Jenkins E. B., Wood B. E., Oliveira C., Blair W. P., Friedman S. D., Gry C., Knauth D., Kruk J. W., Lacour S., Lehner N., Redfield S., Shull J. M., Sonneborn G., Williger G. M., 2006, ApJ, 647, 1106
Loison J.-C., Wakelam V., Hickson K. M., Bergeat A., Mereau R., 2014, MNRAS, 437, 930
Masunaga H., Inutsuka S.-i., 2000, ApJ, 531, 350
Millar T. J., Bennett A., Herbst E., 1989, ApJ, 340, 906
Miyauchi N., Hidaka H., Chigai T., Nagaoka A., Watanabe N., Kouchi A., 2008, Chemical Physics Letters, 456, 27
Mottram J. C., van Dishoeck E. F., Schmalzl M., Kristensen L. E., Visser R., Hogerheijde M. R., Bruderer S., 2013, A&A, 558, A126
Öberg K. I., Fuchs G. W., Awad Z., Fraser H. J., Schlemmer S., van Dishoeck E. F., Linnartz H., 2007, ApJ, 662, L23
Öberg K. I., Linnartz H., Visser R., van Dishoeck E. F., 2009, ApJ, 693, 1209
Öberg K. I., van Dishoeck E. F., Linnartz H., 2009, A&A, 496, 281
Pagani L., Roueff E., Lesaffre P., 2011, ApJ, 739, L35
Parise B., Simon T., Caux E., Dartois E., Ceccarelli C., Rayner J., Tielens A. G. G. M., 2003, A&A, 410, 897
Persson M. V., Jørgensen J. K., van Dishoeck E. F., 2013, A&A, 549, L3
Persson M. V., Jørgensen J. K., van Dishoeck E. F., Harsono D., 2014, A&A, 563, A74
Phillips T. G., Vastel C., 2003, in Curry C. L., Fich M., eds, SFChem 2002: Chemistry as a Diagnostic of Star Formation Future Millimeter/Submillimeter Instrumentation and Science Opportunities: The Example of Deuterated Molecules. p. 3
Pilbratt G. L., Riedinger J. R., Passvogel T., Crone G., Doyle D., Gageur U., Heras A. M., Jewell C., Metcalfe L., Ott S., Schmidt M., 2010, A&A, 518, L1
Pineda J. E., Maury A. J., Fuller G. A., Testi L., García-Appadoo D., Peck A. B., Villard E., Corder S. A., van Kempen T. A., Turner J. L., Tachihara K., Dent W., 2012, A&A, 544, L7
Podio L., Kamp I., Codella C., Cabrit S., Nisini B., Dougados C., Sandell G., Williams J. P., Testi L., Thi W.-F., Woitke P., Meijerink R., Spaans M., Aresu G., Ménard F., Pinte C., 2013, ApJ, 766, L5
Roberts H., Herbst E., Millar T. J., 2003, ApJ, 591, L41
Roberts H., Herbst E., Millar T. J., 2004, A&A, 424, 905
Schutte W. A., Tielens A. G. G. M., Whittet D. C. B., Boogert A., Ehrenfreund P., de Graauw T., Prusti T., van Dishoeck E. F., Wesselius P., 1996, A&A, 315, L333
Semenov D., Hersant F., Wakelam V., Dutrey A., Chapillon E., Guilloteau S., Henning T., Launhardt R., Piétu V., Schreyer K., 2010, A&A, 522, A42
Sipilä O., Caselli P., Harju J., 2013, A&A, 554, A92
Stark R., Sandell G., Beck S. C., Hogerheijde M. R., van Dishoeck E. F., van der Wal P., van der Tak F. F. S., Schäfer F., Melnick G. J., Ashby M. L. N., de Lange G., 2004, ApJ, 608, 341
Taquet V., López-Sepulcre A., Ceccarelli C., Neri R., Kahane C., Coutens A., Vastel C., 2013, ApJ, 768, L29
Taquet V., Peters P. S., Kahane C., Ceccarelli C., López-Sepulcre A., Toubin C., Duflot D., Wiesenfeld L., 2013, A&A, 550, A127
van der Tak F. F. S., Chavarría L., Herpin F., Wyrowski F., Walmsley C. M., van Dishoeck E. F., Benz A. O., Bergin E. A., Caselli P., Hogerheijde M. R., Johnstone D., Kristensen L. E., Liseau R., Nisini B., Tafalla M., 2013, A&A, 554, A83
van Dishoeck E. F., Herbst E., Neufeld D. A., 2013, Chemical Reviews, 113, 9043
Vastel C., Ceccarelli C., Caux E., Coutens A., Cernicharo J., Bottinelli S., Demyk K., Faure A., Wiesenfeld L., Scribano Y., Bacmann A., Hily-Blant P., Maret S., Walters A., Bergin E. A., et al. 2010, A&A, 521, L31
Vastel C., Phillips T. G., Ceccarelli C., Pearson J., 2003, ApJ, 593, L97
Vastel C., Phillips T. G., Yoshida H., 2004, ApJ, 606, L127
Visser R., Doty S. D., van Dishoeck E. F., 2011, A&A, 534, A132
Visser R., Jørgensen J. K., Kristensen L. E., van Dishoeck E. F., Bergin E. A., 2013, ApJ, 769, 19
Whittet D. C. B., 1993, Observations of Molecular Ices. p. 9

APPENDIX A: ABUNDANCES PREDICTED IN THE ICES IN THE FOREGROUND CLOUD

APPENDIX B: ABUNDANCES PREDICTED WITH DIFFERENT VALUES OF THE RATE COEFFICIENT OF THE REACTION $H_2D^+ + H_2 \rightarrow H_3^+ + HD$

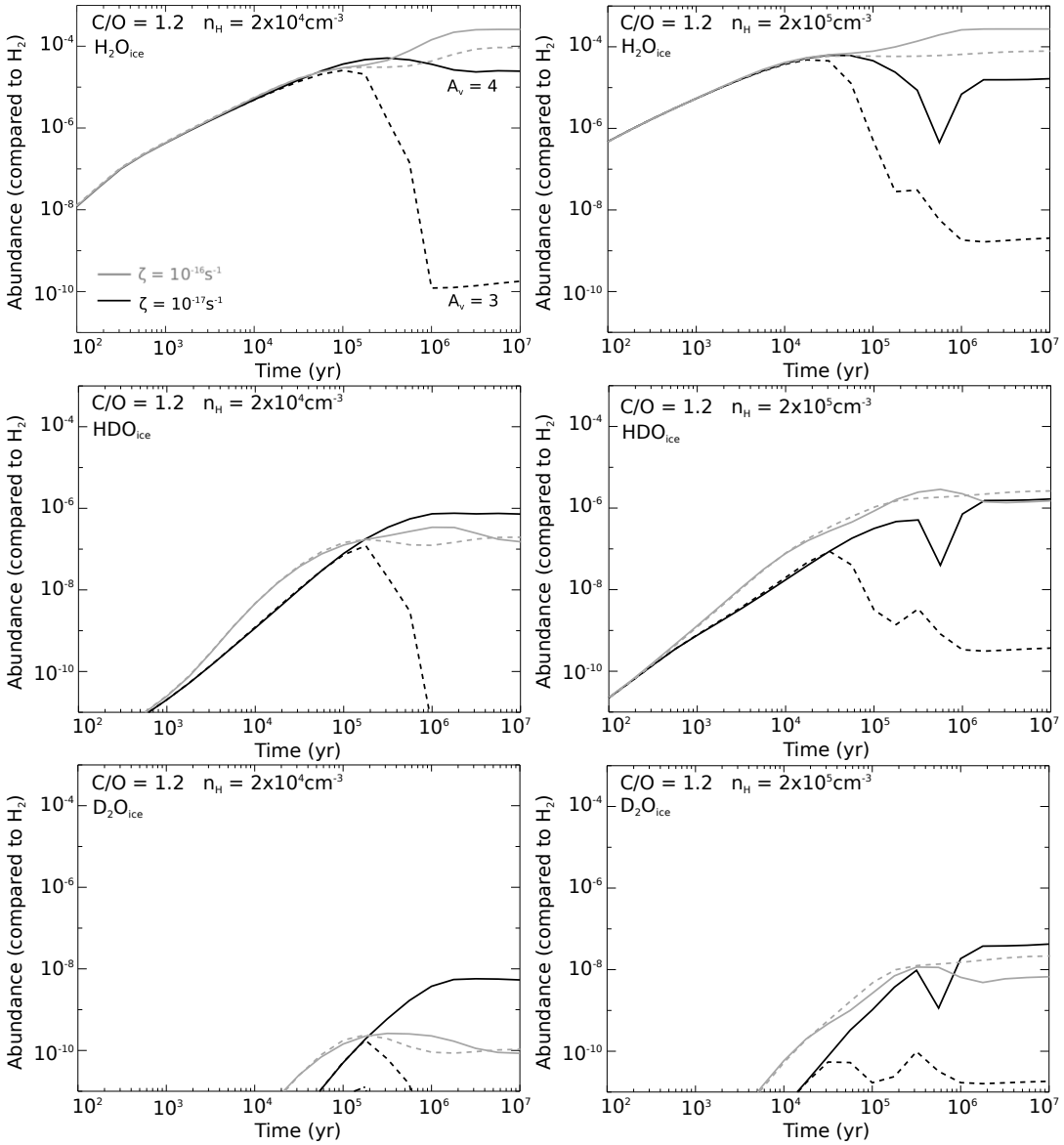

Figure A1. Abundances of H_2O, HDO and D_2O in the ices as a function of time predicted by the model for the foreground cloud. Gas and dust temperature is the same for all models: 15 K. The elemental C/O abundance ratio is 1.2. The left side of the model has been obtained for a total H density of 2×10^4 cm^{-3} and the right side for a total H density of 2×10^5 cm^{-3}. Black curves have been obtained for a cosmic-ray ionization rate ζ of 10^{-17} s^{-1} whereas grey curves have been obtained for a ζ of 10^{-16} s^{-1}. Solid lines represent an A_V of 4 and dashed lines an A_V of 3.

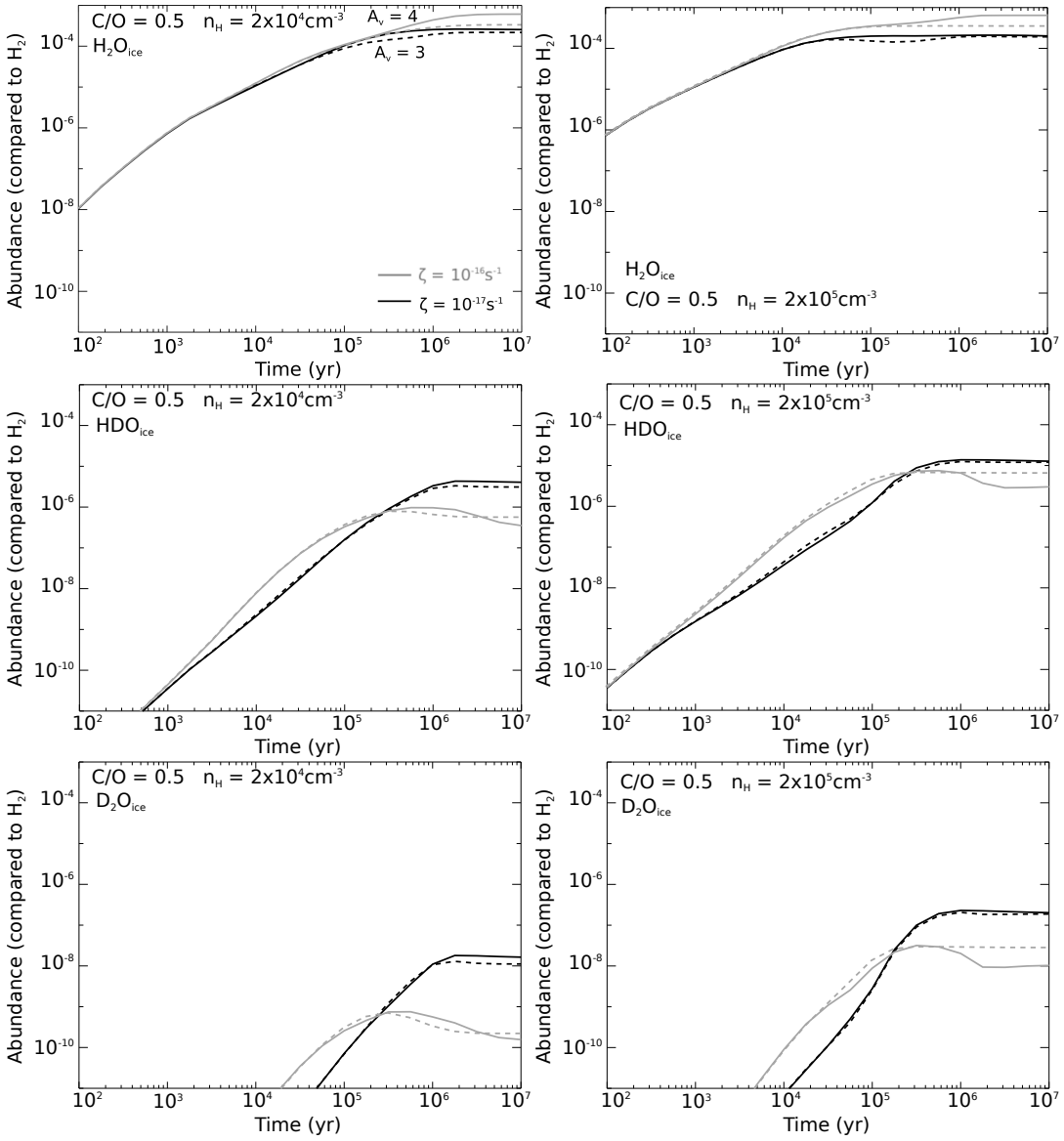

Figure A2. Same as Fig. A1 but a C/O of 0.5.

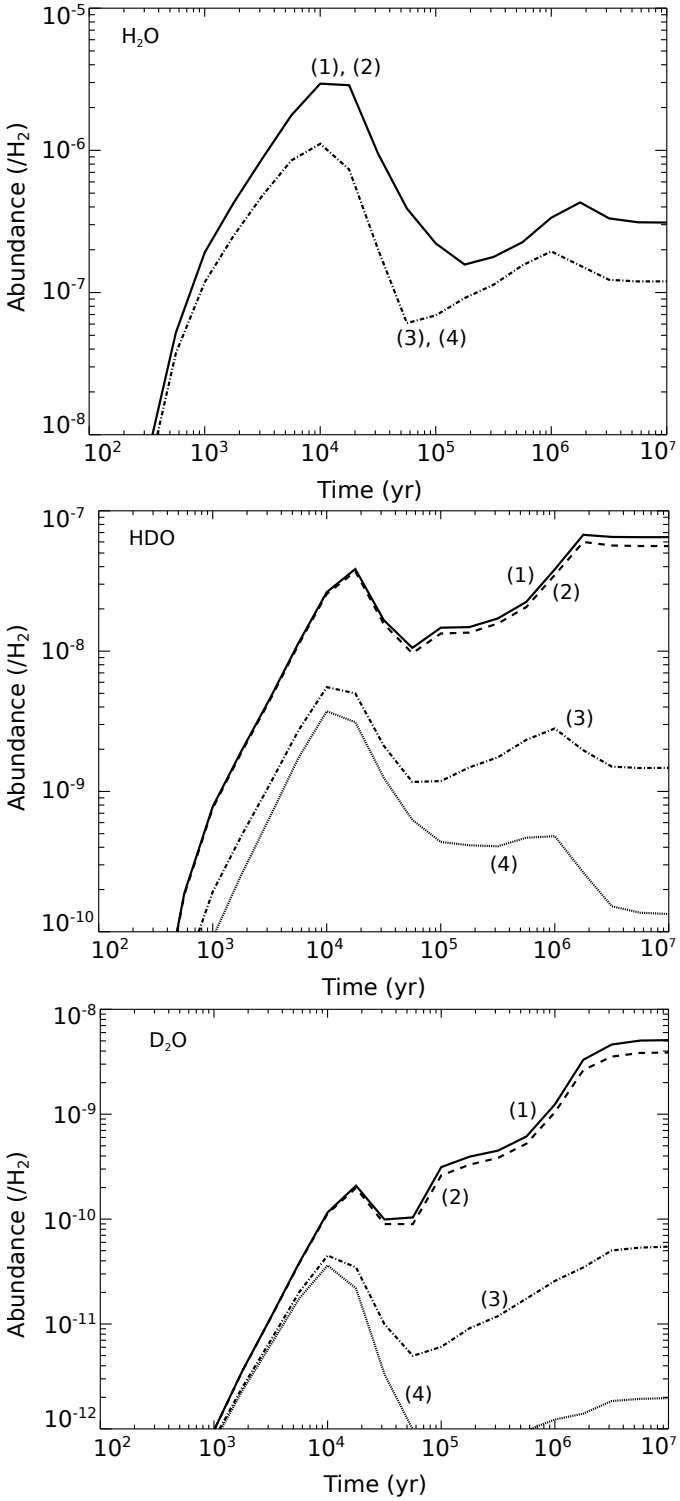

Figure B1. Abundances of H_2O, HDO and D_2O as a function of time, computed in the foreground cloud for different values of the rate coefficient of the reaction $H_2D^+ + H_2 \rightarrow H_3^+ + HD$ mimicking the o/p H_2 ratio of 10^{-3} (curves 2), 0.1 (curves 3) and 3 (curves 4). The reference model, without considering the ortho form of H_2 is shown by curves 1. For these models, the gas and dust temperatures are 15 K, the density is 2×10^5 cm^{-3}, the visual extinction is 4, the C/O elemental ratio is 0.5, and the cosmic-ray ionization rate is 10^{-16} s^{-1}.

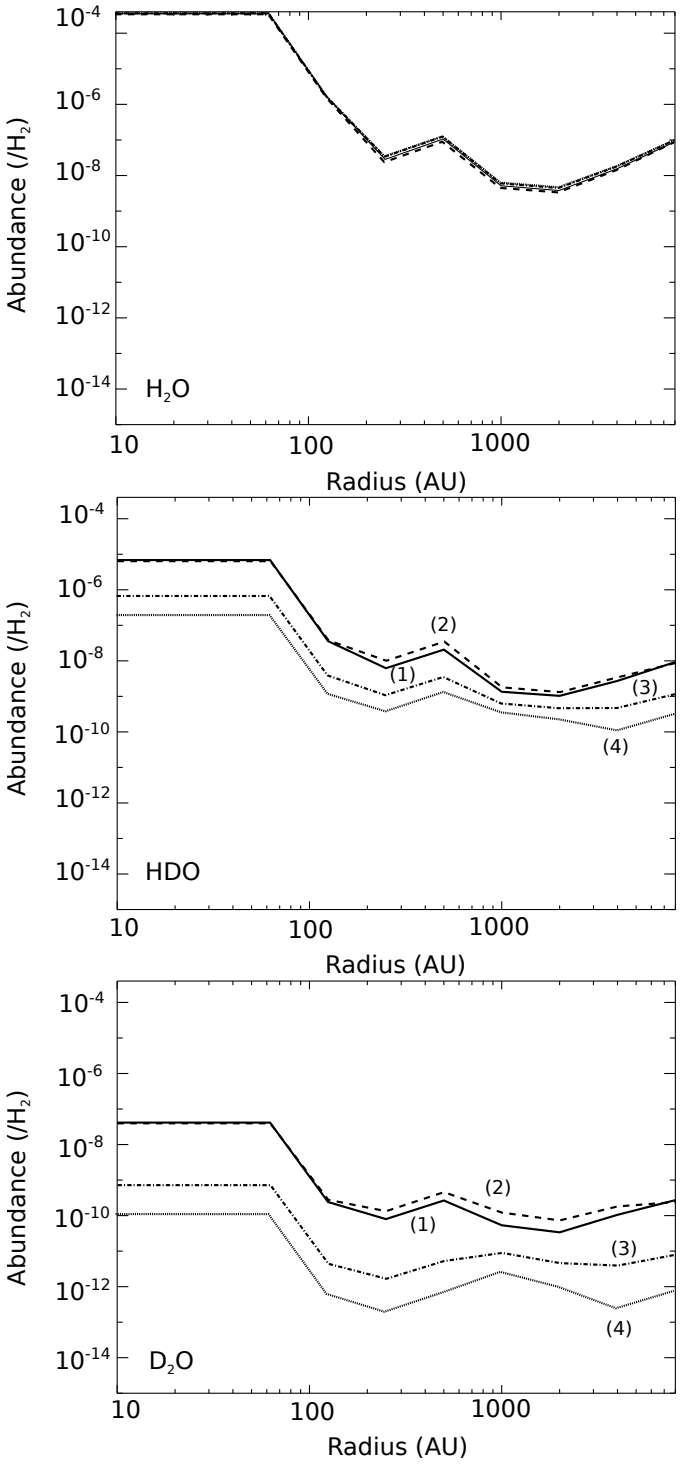

Figure B2. Abundances of H_2O, HDO and D_2O as a function of radius in the protostellar envelope, computed for different values of the rate coefficient of the reaction $H_2D^+ + H_2 \rightarrow H_3^+ + HD$ mimicking the o/p H_2 ratio of 10^{-3} (curves 2), 0.1 (curves 3) and 3 (curves 4). The reference model, without considering the ortho form of H_2 is shown by curves 1. For these models, the C/O elemental ratio is 0.5 and the cosmic-ray ionization rate is 10^{-16} s^{-1}.